ACCSCIENCE PUBLISHING

International Journal of Bioprinting

REVIEW ARTICLE

Hierarchical 3D-printed scaffolds for osteochondral regeneration: From biomimetic design to functional integration

Qi Wang, Wei Zhu, Ruoying Wang, and Xisheng Weng*

Department of Orthopedics, Peking Union Medical College Hospital, Chinese Academy of Medical Sciences & Peking Union Medical College, 100730 Beijing, China

(This article belongs to the *Special Issue: Advances in Bioprinting and Organ-on-a-chip and Applications for Precision Medicine*)

Abstract

Osteochondral defects, characterized by the structural and functional disruption of articular cartilage and subchondral bone, present significant clinical challenges due to the tissue's limited intrinsic regenerative capacity. Scaffold-based tissue engineering has paved the way for osteochondral defect treatment; however, fully restoring the complex structure and composition of native osteochondral tissue remains challenging. Recent advances in three-dimensional (3D) printing have enabled the fabrication of layered, anisotropic scaffolds designed to biomimetically recapitulate the native tissue's zonal properties through precise hierarchical design. High-resolution fabrication techniques facilitate the construction of delicate microarchitectures, while advanced bioprinting methods allow for the incorporation of bioactive factors and cells into the scaffold matrix. This review emphasizes the following four scaffold design paradigms: composite gradients, microarchitectural patterning, biochemical gradients, and cellular heterogeneity. Moreover, key properties of multilayered scaffolds are discussed, including mechanical performance, interfacial strength, and degradation behavior. In addition, several obstacles associated with the *in vivo* scaffold application are discussed, providing insights to guide future clinical translation in osteochondral defects treatment.

Keywords: 3D-printed scaffold; Biomaterials; Osteoarthritis; Osteochondral regeneration; Regenerative medicine; Tissue engineering

***Corresponding author:**
Xisheng Weng
(xshweng@medmail.com.cn)

Citation: Weng X, Wang R, Zhu W, Wang Q. Hierarchical 3D-printed scaffolds for osteochondral regeneration: From biomimetic design to functional integration. *Int J Bioprint*. 2025;11(4):4-31. doi: 10.36922/IJB025120100

Received: March 22, 2025
Revised: April 16, 2025
Accepted: April 28, 2025
Published online: April 28, 2025

1. Introduction

Osteochondral defect, caused by injury or various forms of arthritis including osteoarthritis (OA), imposes a growing global health burden.[1,2] Over 500 million individuals worldwide are suffering from OA,[3] making it the seventh leading cause of disability.[4] Notably, early-onset OA (diagnosed before the age of 55) accounts for over 50% of new cases,[5] indicating a growing trend of osteochondral injuries occurring in younger populations. Unfortunately, osteochondral tissue has limited self-healing capability due to cartilage avascularity.[6] Current therapeutic approaches include the following: (1) palliative treatment, such as topical or oral administration of non-steroidal anti-inflammatory drugs (NSAIDs), corticosteroid intra-articular injections, or physical

therapy for symptom relief[7]; (2) microfracture surgery, a minimally invasive option for defects less than 2 cm^2 via marrow stimulation[8]; (3) autologous or allogeneic grafts, which are limited by insufficient tissue availability and poor integration between the graft and host tissue[9]; and (4) total knee joint arthroplasty (TKA), commonly used to treat end-stage joint degeneration, but in younger patients associated with major drawbacks, including limited lifespan of the prosthesis, restricted physical function and the risk of future revision surgeries.[10-12]

Currently, conventional treatments have proven insufficient to achieve complete bone and cartilage regeneration. In recent years, 3D-printed scaffolds have been increasingly utilized for *in situ* regeneration of joint defects. Considering the layered characteristics of articular cartilage, 3D-printed hierarchical biomimetic scaffolds have garnered significant attention. This paper aims to review the recent advancements in gradient-manufactured strategies based on 3D printing, providing a novel approach for cartilage repair.

2. Natural gradient of osteochondral tissue

Native articular cartilage is a complex hierarchical tissue that transitions from a surface layer of hyaline cartilage, continuing with calcified cartilage in the deep layer, then to the subchondral osseous layer. These layers account for 90%, 5%, and 5% of the total thickness, respectively.[13] Each layer has a distinct composition, along with different microenvironment and mechanical properties. This hierarchical structure enables the joint to bear loads and serves to distribute load, absorb shock, and facilitate motion.[14]

From the surface of the articular cartilage to the subchondral bone, the structure is divided into several distinct layers: the superficial zone (SZ), middle zone (MZ), deep zone (DZ), calcified cartilage zone (CCZ), and subchondral bone (SCB). These layers not only differ in depth but also exhibit gradient features in various aspects, including composition, biochemical properties, mechanical characteristics, and topography gradient.

2.1. Content gradient

Hierarchical compositional gradients emerge across zones from the SZ to the SCB. Collagen types I/II/X, glycosaminoglycans (GAGs), proteoglycans, water, and hydroxyapatite demonstrate depth-dependent gradients, with systematic redistribution patterns.[15]

In the SZ, collagen type II exhibits lower concentration but forms densely packed, surface-parallel fibrillar networks, providing shear resistance to the surface. Progressing to the MZ, fibers adopt a loosely organized configuration, facilitating stress distribution through enhanced deformability. Collagen type II reaches maximal concentration in the DZ, with vertically oriented fibrillar bundles optimized for compressive load-bearing.[16] The CCZ undergoes a compositional shift, replacing collagen type II with type X to establish a calcified matrix for osteochondral integration.[17] This transition reverses abruptly in the SCB, where collagen type I supersedes type X as the predominant isoform. While minimally expressed in the CCZ, collagen type I becomes the dominant organic constituent in the SCB, conferring structural rigidity and tensile strength.[16]

GAGs and proteoglycans increase progressively from the SZ to the DZ, peaking in the DZ. This gradient facilitates water retention and hydrostatic pressure management, critical for load-bearing.[18] Their levels drop sharply in the CCZ as the matrix undergoes mineralization.

Water content is the highest in the SZ,[16] aiding lubrication and reducing friction. It decreases progressively through the MZ and DZ, where lower levels enhance structural strength. In the CCZ, water is nearly absent due to the predominance of mineralized matrix.

Hydroxyapatite concentration increases steadily within the CCZ, reaching its peak in the SCB. This gradient provides hardness and compressive strength to the mineralized regions.[16]

These gradient distributions ensure a seamless mechanical and structural transition between cartilage and bone, supporting the functional integrity of the joint.

2.2. Biochemical gradient

The extracellular matrix (ECM) creates a specialized microenvironment that supports tissue metabolism, repair, and growth, mediated by biomolecular factors such as transcription factors, cytokines, and signaling molecules.[19] Gene expression regulated by these factors varies across osteochondral layers, with zone-specific markers supporting the specialized functions of each region. Articular cartilage and subchondral bone exhibit distinct molecular biology profiles that support their specialized functions. In the SZ, key biomolecular factors such as aggrecan, collagen type II alpha-1 chain (COL2A1), and SOX9 display peak expression levels. Aggrecan and COL2A1 are critical for maintaining cartilage mechanical integrity, while SOX9 regulates chondrocyte differentiation and maturation.[20] Moving to the MZ and DZ, these factors decrease, reflecting a shift from cartilage synthesis to mineralization processes. Concurrently, bone morphogenetic protein-2 (BMP2) and collagen type X alpha-1 chain (COL10A1) are upregulated, driving chondrocyte differentiation into osteoblast-like progenitors[21] and promoting matrix calcification.[22] Alkaline

phosphatase (ALP), a key enzyme in mineralization, is selectively enriched in these zones, underscoring their role in cartilage maintenance and mineralization.[23]

In the CCZ, osteogenesis factors like COL10A1, ALP, and Runx2 are most highly expressed.[24] Runx2, a key osteogenic transcription factor, drives the transition of hypertrophic chondrocytes into osteoblast-like cells, facilitating ossification. Vascular endothelial growth factor (VEGF), a critical angiogenic factor, ensures vascular invasion, necessary for bone formation.[25] These gradients promote the mineralization and ossification of the cartilage matrix, thereby bridging cartilage and bone.

In the SCB, factors like osteocalcin, osteopontin (OPN), Receptor Activator for Nuclear Factor-κ B Ligand (RANKL), and matrix metalloproteinases (MMPs) are concentrated, reflecting bone mineralization, remodeling, and resorption.[26,27] Osteocalcin and OPN are involved in bone matrix formation, while RANKL regulates osteoclast differentiation for bone resorption. MMPs, key for ECM turnover, are highly expressed in the SCB, where active bone remodeling occurs.[28,29] The distribution of osteochondral substances is listed in Table 1.

2.3. Mechanical gradient

The mechanical properties of cartilage layers exhibit a depth-dependent pattern,[30] with each stratum fulfilling specialized biomechanical functions that correlate with the compositional gradients and microstructural organizations described in **Section 2.1**. The SZ, characterized by the lowest compressive modulus, maintains joint flexibility through its unique architecture: fine fibers of collagen types II/IX aligned parallel to the articular surface,[30] coupled with densely packed, flattened disc-shaped chondrocytes arranged horizontally,[2] collectively create a low-friction interface that minimizes shear stress. The MZ exhibits transitional viscoelastic properties, enabled by its randomly oriented thicker collagen bundles forming a porous scaffold, where sparsely distributed spherical chondrocytes facilitate stress redistribution and energy dissipation. The DZ achieves maximal compressive resistance through perpendicularly aligned hypertrophic collagen fibrils relative to the articular surface, accompanied by spherical chondrocytes organized into columnar arrays parallel to the collagen orientation. The CCZ demonstrates ultimate stiffness through mineralized collagen networks, firmly anchoring the cartilage to the SCB while preventing mechanical delamination.[6] This hierarchical mechanical stratification, evolutionarily conserved across mammalian articular cartilage systems, enables efficient stress transmission through depth-specific structural adaptations, ensuring optimal joint functionality and biomechanical stability.

Table 1. Gradient distribution of biochemical factors in articular cartilage

Substance	Function	Distribution
Aggrecan	Enhances cartilage strength and elasticity	High in SZ; low in DZ
COL2A1	Provides cartilage structural integrity	High in SZ; decreases toward CCZ
SOX9	Maintains chondrocyte phenotype	Predominantly active in SZ; reduced in deeper layers
TGF-β	Regulates cell proliferation and ECM synthesis	High in MZ; lower in deeper layers
BMP2	Promotes chondrocyte-to-osteoblast differentiation	Low in SZ and MZ; high in DZ and CCZ
COL10A1	Marker of cartilage mineralization	Present in DZ; high in CCZ
ALP	Promotes mineralization	High in DZ and CCZ
VEGF	Promotes angiogenesis	High in DZ; present in CCZ
Runx2	Promotes cartilage-to-bone conversion	Highest in CCZ
Osteocalcin	Involved in bone mineralization	Present in SCB; high in CCZ
OPN	Involved in bone mineralization and cell adhesion	High in SCB
RANKL	Stimulates osteoclast differentiation	High in SCB
MMPs	Degrades ECM components; aids in tissue remodeling	High in SCB

Abbreviations: ALP, alkaline phosphatase; BMP2, bone morphogenetic protein-2; COL2A1, collagen type II alpha-1 chain; COL10A1, collagen type X alpha-1 chain; CCZ, calcified cartilage zone; DZ, deep zone; ECM, extracellular matrix; MMPs, matrix metalloproteinases; MZ, middle zone; OPN, osteopontin; RANKL, receptor activator of nuclear factor-κB ligand; SCB, subchondral bone; SZ, superficial zone; TGF-β, transforming growth factor β; VEGF, vascular endothelial growth factor.

Niu et al.[31] quantified depth-dependent mechanical gradients in rabbit articular cartilage, reporting Young's modulus progression from the SZ (0.4–0.6 MPa) through the MZ (0.6–1.0 MPa) to the DZ (2.0–3.0 MPa). This mechanical gradient was corroborated in porcine cartilage by Sun et al.,[32] who documented analogous depth-related variations with SZ (0.8 MPa), MZ (2.0 MPa), and DZ (3.6 MPa) Young's modulus values.

The mechanically vulnerable regions within cartilage tissue also correspond to distinct histological microstructural features. A distinct calcified cartilage band, referred to as the "tidemark," separates the DZ from the CCZ, marking the mineralization front of the calcified cartilage. Continuous collagen fibrils pass through the tidemark, hence serving as a transitional interface between calcified and non-calcified cartilage and facilitating the gradual transition of tissue mineralization.[33] The boundary between the CCZ and the SCB is demarcated by the "cement line." The absence of continuous collagenous connections between the CCZ and the SCB renders this region biomechanically vulnerable.[34].Furthermore, the pronounced stiffness changes between the CCZ and SCB are hypothesized to be a key factor underlying the delamination of cartilage from the bone, particularly under shear stress conditions.[35] This steep variation in mechanical properties creates localized stress concentrations, exacerbating the risk of tissue failure at the cartilage–bone interface.[36]

The progression of OA is characterized by progressive reductions in both elastic modulus and stiffness of articular cartilage.[37] Emerging evidence suggests that early-stage OA may involve biomechanical precursors, including stiffening of the DZ and diminished SCB stiffness, prior to overt cartilage degeneration.[38] Furthermore, the elastic modulus of cartilage demonstrates a significant correlation with OA severity grades.[39] Quantitative analyses reveal substantial mechanical degradation in advanced OA, exemplified by the SZ Young's modulus reduction from 26.51 ± 10.63 MPa in healthy cartilage to 18.58 ± 9.61 MPa in severe OA specimens. Concurrently, both aggregate modulus and shear modulus exhibit significant decreases in moderate-to-severe OA, particularly within the SZ and MZ, indicative of compromised load-bearing capacity.[40]

3. Hierarchy establishment strategies for osteochondral regenerating scaffold

Over the past decade, hierarchical 3D-printed scaffolds have emerged as a predominant strategy for osteochondral regeneration. Advances in fabrication technologies have spurred the development of multiphase design strategies to mimic zonal tissue complexity. Hierarchical 3D printing strategies are systematically categorized as follows (Figure 1): (1) composite gradient defined as methodologies that achieve stratified functionality through layer-specific variations in material composition and physicochemical properties; (2) microarchitectural gradient characterized by the implementation of function-specific structural configurations across distinct layers to regulate anisotropic mechanical or nutrient transport behaviors; (3) biochemical gradient entailing spatio-temporal control of biochemical factors within layered constructs to achieve zonal biological responses; and (4) cell heterogeneity involving heterogeneous seed cell populations within discrete strata to emulate native tissue. Recent research efforts have focused on optimizing these hierarchical architectures, with key zone-specific fabrication approaches systematically categorized in Table 2.

3.1. Composite gradient

Composite gradient architectures have become a predominant methodology for engineering scaffold hierarchical organization. This paradigm employs biphasic or multiphasic systems integrating distinct biomaterials, each engineered to address zone-specific mechanical and functional demands. Typical designs incorporate the following: (1) a bioactive, elastomeric, and porous phase for chondral regeneration; and (2) a mechanically reinforced, slow-degrading phase replicating subchondral bone properties.

Materials commonly used for the chondral layer include natural biomaterials such as collagen, hyaluronic acid (HA),[65] sodium alginate (SA),[66] agarose,[67] cellulose,[41] and silk fibroin (SF).[68] These natural materials provide an optimal environment for cell adhesion, proliferation, and growth. However, their mechanical and physicochemical properties may not always be sufficient for tissue engineering applications, leading to the increased use of synthetic materials like polyethylene glycol (PEG),[69] polycaprolactone (PCL), polylactic acid (PLA),[70] gelatin methacrylate (GelMA),[71] and polyethylene glycol diacrylate (PEGDA).[43] These synthetic materials can be modulated during the synthesis process to achieve desired properties. Despite superb mechanical properties, they lack integrin-binding ligands, which limits direct interaction with cells.

Ceramic materials, which are inorganic and non-metallic, are typically characterized by their superb hardness and brittleness. Notable ceramic materials used for osteochondral regeneration include hydroxyapatite (HAp),[72] biphasic calcium phosphate (BCP),[73] tricalcium phosphate (TCP),[57] and bioactive glass (BG).[41] They exhibit favorable biocompatibility and porosity, promoting cell infiltration and tissue integration.[41] Furthermore, inorganic ions released by ceramic materials, such as silicon (Si), lithium (Li), and magnesium (Mg) ions, can

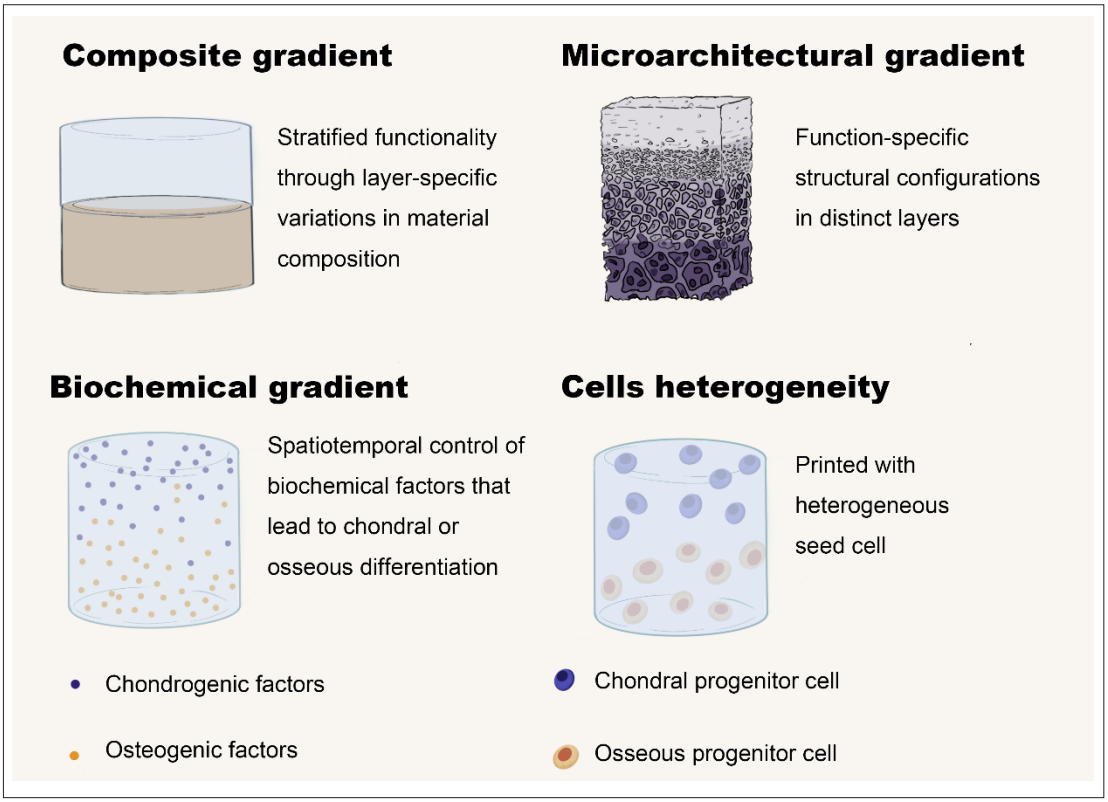

Figure 1. A schematic diagram of natural gradient classification for osteochondral tissue.

promote osteochondral regeneration. Li ions have been shown to stimulate chondrogenesis by upregulating exosomal miR-455-3p in bone marrow mesenchymal stem cells (BMSCs).[74] Mg ions and Mg transporter subtype 1 protein (MagT1) enhance osteogenic differentiation in rBMSCs.[75] Si ions promote angiogenesis by modulating the expression of insulin-like growth factor-1 (IGF-1) and VEGF.[76] However, the use of ceramic materials is limited due to their asynchronized degradation relative to bone regeneration.[77]

Due to the zonal mechanical strength of normal cartilage, which is adapted to different functions, providing layered mechanical support during the repair process and achieving biomimetic repair outcomes are crucial. It has long been established that the growth of both cartilage and bone tissues, both *in vivo* and *in vitro*, is influenced by the surrounding mechanical strength.[78,79] Cells can sense and respond to variations in substrate stiffness, thereby regulating their diffusion, proliferation, and gene expression.[80] Yang et al.[81] fabricated HAp and PEG/SF composites with different stiffness levels and induced osteogenesis in rBMSCs, revealing a positive correlation between stiffness and the expression of osteogenic markers. Cao et al.[82] demonstrated that the matrix stiffness-sensitive miR-99b regulates the osteogenic and adipogenic differentiation of BMSCs by targeting the rapamycin signaling pathway. Similarly, Lai et al.[83] demonstrated that substrate stiffness modulates BMSCs proliferation via exosome-mediated mechanotransduction through Yes-associated protein (YAP) pathways.

Scaffolds with a lower elastic modulus (~10 MPa) inhibit the regeneration of the SCB while promoting the formation of fibrous tissue at the articular interface. In contrast, scaffolds with a higher elastic modulus (~1000 MPa) may compress the opposing cartilage, leading to its degradation.[84] Consequently, scaffolds with biphasic mechanical properties have been extensively studied to improve the healing of both bone and cartilage. Diloksumpan et al.[45] developed a triple-layer scaffold using extrusion-based printing and melt electrospinning writing (MEW). The top chondral layer consists of a PCL mesh infused with GelMA hydrogel, while the middle layer, composed of a PCL mesh and polymer-calcium phosphate (PCaP) composite, is designed to replicate the structure of calcified cartilage for chondral-osseous transition. The osseous layer is fabricated from PCaP. Each layer was designed to adapt to its specific mechanical demand. Gao et al.[47] established a bilayer scaffold based on GelMA, where

the osseous layer was optimized by incorporating HA into the GelMA matrix, thereby enhancing the compressive modulus for bone formation.

3.2. Microarchitectural gradient

Native cartilage exhibits a gradient in microarchitectural patterning, encompassing variations in geometry, porosity, stiffness, and density,[85] which are essential for maintaining its mechanical properties, as described in **Section 3.2**. Meanwhile, the porous structure plays a crucial role in cell adhesion, metabolism, and proliferation, which are critical for spatial organization and tissue regeneration in tissue engineering. Conventional fabrication techniques—such as solvent casting, freeze-drying, electrospinning, and gas foaming—can produce well-structured scaffolds, yet they lack precise microstructural control. Key factors include pore size,[60] shape, distribution,[61] and density.[86] In contrast, 3D printing offers a highly adaptable approach for designing scaffolds that closely replicate the native cartilage microarchitecture.

Previous studies have demonstrated that neo-tissue regeneration predominantly initiates at the defect periphery, whereas central regions often exhibit compromised regeneration capacity due to reliance on cellular migration through the scaffold matrix.[87] Proper microstructures (e.g., pores or channels) provide mechanical support and guidance for cell migration,[88] while simultaneously facilitating nutrient transportation and bioactive factor release. Gu et al.[61] developed a biomimetic bilayer scaffold using digital light processing (DLP)-based 3D printing. The upper cartilage layer features a "lotus and radial" pore distribution that facilitates the transverse migration of chondrocytes and cartilage progenitor cells at superficial layers. The bottom osseous layer exhibits a "lotus" pore structure, guiding BMSCs to vertically migrate to the defect site, thus creating a native tissue-like cell distribution pattern. *In vitro* experiments demonstrated a preference for cell migration along the delicate "lotus and radial" pore structure (Figure 2), resulting in nearly a fourfold increase in cell migration compared to non-porous scaffolds.

Microarchitectural features of biomaterials also regulate cell differentiation.[89,90] Events such as cell–cell interactions, adhesion molecule binding, gap junction formation, and cytoskeletal reorganization, significantly impact chondrogenic differentiation.[91,92] Larger pore sizes promote the aggregation and proliferation of MSCs, facilitating chondrogenic condensation.[60] Li et al.[93] demonstrated that pore sizes in 3D-printed silica hybrid scaffolds critically regulate human BMSCs (hBMSCs) lineage commitment: pores of ~100 μm resulted in poor matrix formation, ~220 μm promoted hyaline cartilage formation through predominant collagen type II deposition, while ~500 μm triggered fibrocartilaginous commitment characterized by collagen type I dominance. Pore sizes around 200 μm promote the maintenance of a spherical cell morphology, facilitating cell–cell interactions, whereas, larger pore sizes encourage cell attachment, reducing intracellular contact. Conversely, smaller pores may not provide sufficient space for ECM production. It has been reported that spherical-shaped BMSCs correlate with higher expression of chondrogenic molecular markers and are more likely to undergo chondrogenic differentiation.[94]

Sun et al.[60] further revealed that pore size modulates BMSCs differentiation by activating the Hypoxia-inducible factor 1α/Focal Adhesion Kinase (HIF1α/FAK) signaling axis. A layered-mesh structured, BMSCs-laden PCL scaffold was fabricated, in which the superficial small-pore zone (SPZ, 150 μm) provides lubrication and shear resistance, while the deep large-pore zone (LPZ, 750 μm) enhances elasticity and maintains structural rigidity. The SPZ exhibited high HIF1α expression, promoting chondrogenesis and maintaining a hyaline cartilage phenotype, whereas the LPZ favored osteogenesis and increased vascularization (Figure 3).

3.3. Biochemical gradient

In scaffold-based osteochondral defect repair, biomimetic strategies for cell-free scaffolds involve *in situ* tissue regeneration through precise coordination of MSC recruitment, differentiation, and maturation. For cell-laden scaffolds, directing cells to undergo specific differentiation at various layers is equally crucial for successful repair. Thus, biochemical factors, functioning as chemoattractants, need to be applied in a spatially distributed manner to regulate cell behavior and optimize tissue regeneration.[95]

Biochemical gradient strategies involve adding growth factors or small molecules to induce cell differentiation. These can be incorporated directly into the material for bioprinting or delivered through carriers such as exosomes or nanoparticles. Additionally, decellularized ECM (dECM) is used to create biochemical gradients.

Growth factors are a large family of cytokines that regulate cell migration, adhesion, proliferation, and differentiation. For cartilage, transforming growth factor (TGF)-β1, IGF-1, fibroblast growth factor-2 (FGF-2), and BMP-2 support maturation and formation, while BMPs, IGF-1/2, TGF-β, and FGFs are primarily involved in bone regeneration.[96] These growth factors are spatially distributed and function in a coordinated manner, working synergistically to promote tissue development and repair. Ding et al.[52] developed a hydrogel scaffold covalently functionalized with bioactive TGF-β1 binding peptides (TBP) to recruit endogenous TGF-β1, thereby

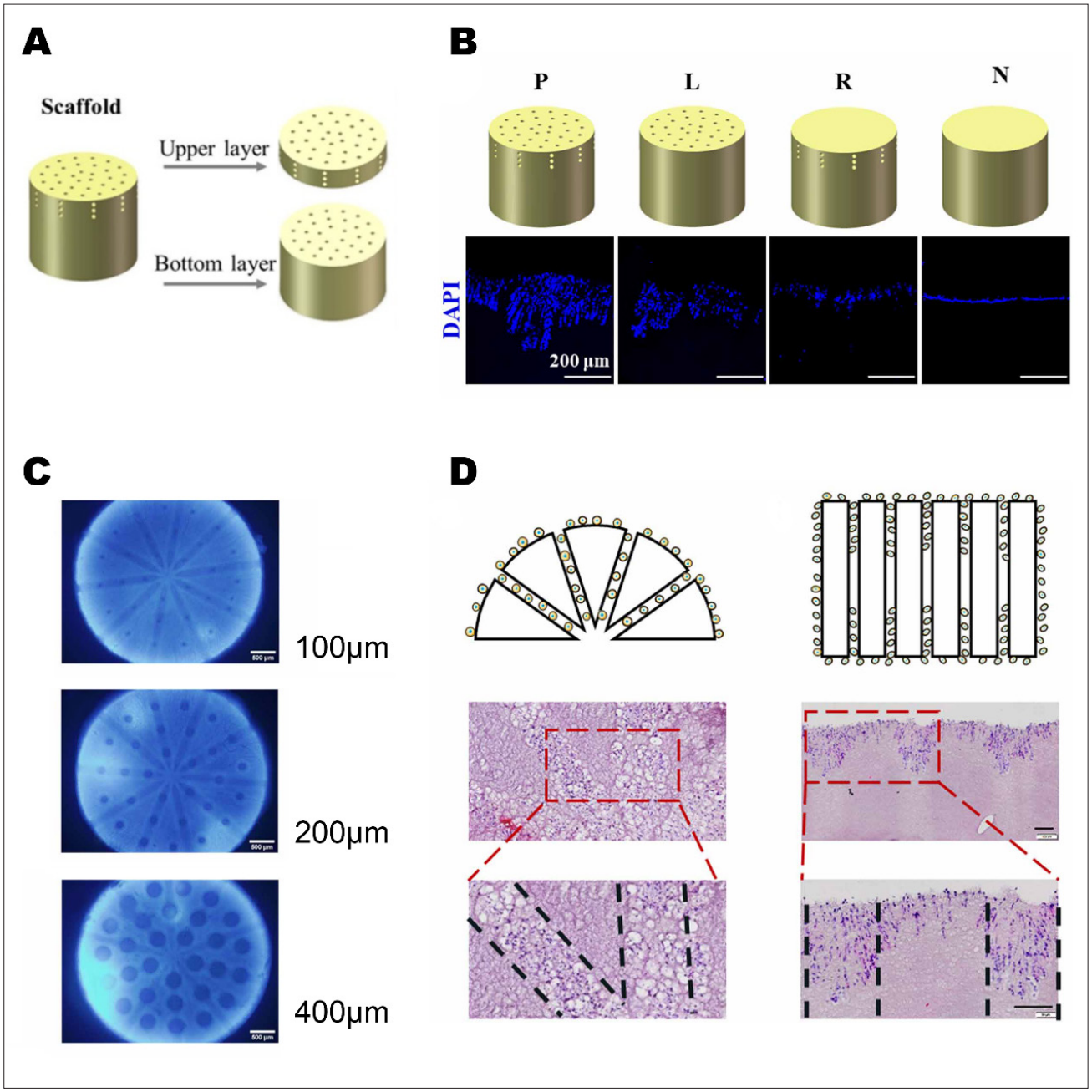

Figure 2. Evaluation of cell infiltration in bilayer scaffolds with different pore architectures. (A) Schematic design of the bilayered scaffold. (B) Representative fluorescent images (DAPI staining) showing cell infiltration into scaffolds 5 days after subcutaneous implantation *in vivo* (scale bar = 200 μm). (C) Fluorescent images of bilayer scaffolds with different longitudinal pore sizes. (D) Schematic illustration and H&E staining images of the P group scaffold in horizontal (left) and vertical (right) sections (scale bar = 100 μm). Black dashed lines indicate pore boundaries in the magnified views. Among all groups, the P group exhibited the greatest cell infiltration depth and the highest number of infiltrating cells, indicating that the combined pore architecture most effectively facilitates cell migration into the scaffold. Group definitions: P = lotus + radial pores; L = lotus pores only; R = radial pores only; N = non-porous scaffold. Reproduced from Ref.[61], Biofabrication (2024), with permission from IOP Publishing.

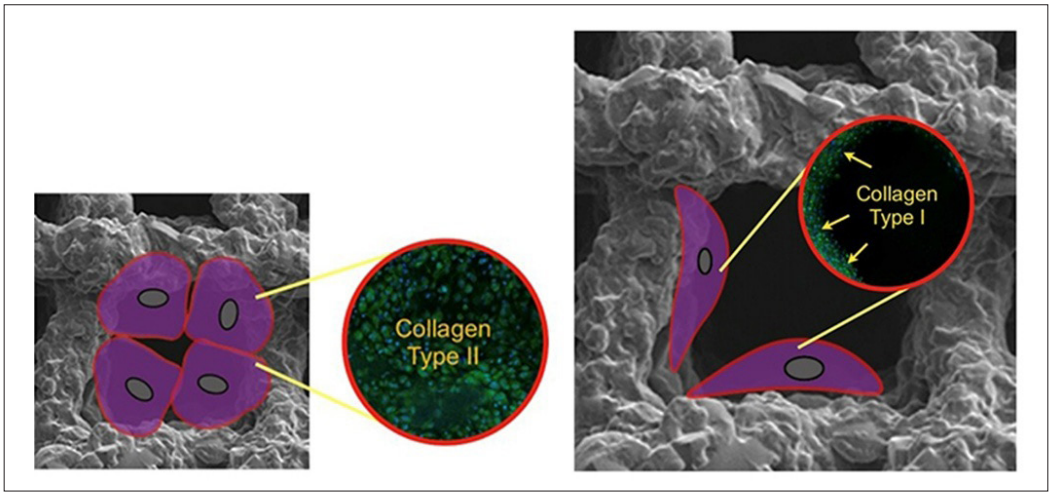

Figure 3. Effect of scaffold pore size on cell morphology and differentiation. hBMSCs cultured in 3D-printed silica hybrid scaffolds exhibited different morphologies depending on the channel size. In scaffolds with smaller channel sizes (~230 μm), cells showed a rounded morphology and underwent chondrogenic differentiation, with widespread expression of type II collagen matrix indicating a hyaline cartilage phenotype. In contrast, in scaffolds with larger pores (~500 μm), cells adopted a spindle-shaped morphology and predominantly expressed type I collagen, suggesting fibrocartilage formation. Reproduced from Ref.[93] with permission from the Royal Society of Chemistry.

enhancing cartilage regeneration. Similarly, Kilian et al.[62] introduced a core-shell bioprinting strategy to fabricate a bilayer scaffold. The chondral layer consists of a human chondrocyte (hChon) shell surrounding a TGF-β3 core, while the osseous layer comprises a human osteoblast (hOB) shell encapsulating a BMP-2 core. This core-shell system enables the spatially controlled delivery of specific cell types and differentiation factors within distinct compartments of the hydrogel strands, promoting targeted tissue regeneration.

The dECM, derived from human or animal tissues, is another biochemical gradient strategy widely used in tissue engineering. It primarily contains ECM macromolecules.[97] The decellularization process preserves the physicochemical signals and biological properties of native tissue, providing a native-like microenvironment that supports the migration, proliferation, and differentiation of BMSCs. Studies have shown that BMSCs embedded in cartilage dECM (DCM) or bone dECM (DBM) hydrogels interact with the adjacent matrix, promoting chondrogenic or osteogenic differentiation and subsequent tissue maturation. However, the mechanical properties of dECM are suboptimal due to the loss of native tissue topography during the decellularization process,[98,99] resulting in delamination, which hinders its application in larger cartilage defect regeneration. Zhang et al.[42] developed a bilayer scaffold using dECM as bioink and enhanced its mechanical properties with SF. The DCM and DBM layers were modified with TGF-β1 and BMP-2, respectively. This scaffold demonstrated promising osteochondral regeneration, exhibiting suitable mechanical strength and degradation rates at the same time. Furthermore, Joyce et al.[100] reinforced an ECM-derived collagen-hyaluronic acid (CHyA) matrix with a 3D-printed PCL framework to enhance mechanical strength to adapt to physiological loads. The PCL reinforcement increased the compressive modulus of the CHyA matrix threefold, which aligned with the physiological range (0.5–2.0 MPa) of healthy cartilage. It also improved the tensile modulus and allowed for suture fixation to the subchondral bone, thereby enhancing scaffold-bone integration. *In vitro* study demonstrated that MSCs were successfully infiltrated the scaffold, leading to significantly higher expression of sGAG.

Small molecules are widely applied in osteochondral engineering to induce cell differentiation, regulate osteoblast/osteoclast function, or exert anti-inflammatory effects. Kartogenin (KGN), which promotes chondrocyte differentiation in a dose-dependent manner,[101] provides a feasible approach to establish biochemical gradients. Wei et al.[55] developed an osteochondral scaffold embedded with BMSCs, exhibiting a high concentration of KGN in the chondral layer and a low concentration of KGN with β-TCP in the osseous layer. Dexamethasone, another small synthesized glucocorticoid molecule,[102] can promote osteogenesis and chondrogenesis by stimulating MSC differentiation into osteoblasts and chondrocytes via Wnt/β-catenin and TGF-β pathways. Its anti-inflammatory properties reduce inflammation, aiding tissue healing. Barrera et al.[103] developed a biomimetic surface coating for implants, applying a layer-by-layer technique to create

Table 2. Hierarchical strategies for 3D-printed osteochondral scaffolds

Scaffold design	Strategy	Seed cell	Manufacturing method	Mechanical properties	*In vivo* model	Reference
wCartilage: Pure cellulose ink Osseous: 58S BG-filled cellulose ink	Composite	Cell-free	Extrusion-based printing	Tensile strength: 5.22 MPa Fracture energy: 1.81 MJ/m^3 Compressive strength: 11.8 MPa	Rabbit	[41]
Cartilage: DCM/SF-TGF-β1 Osseous: PCL + DBM/SF-BMP2	Composite biochemical	BMSCs	Extrusion-based printing	Compressive stress: 44 kPa (cartilage), 47 kPa (osseous without PCL), 310 kPa (osseous with PCL) CM: 9-fold enhancement with PCL applied	Rabbit	[42]
WWCartilage: PCL-HAp Osseous: PHA + PEGDA + DVC	Composite	Cell-free	Extrusion-based printing	YM: 269 ± 20 MPa (PCL), 67% increase in PCL-HAp Flexural stiffness: 206% increase in PCL-HAp (compared to PCL)	Goat	[43]
Cartilage: SA-dNC-$CaCl_2$ Osseous: SA-GelMA-nHA- $CaCl_2$	Composite	Cell-free	Extrusion-based printing	CM: 94.64 ± 5.27 kPa (G-dNC/nHA), 89.12 ± 15.2 kPa (G-nHA control), 70.55 ± 4.29 kPa (G-control) Shear strength: maximum in G-dNC/nHA G: Gradient	Rat	[44]
Cartilage: PCL mesh + GelMA Intermediate: MEW mesh + PCaP Osseous: PCaP	Composite	BMSCs	MEW + extrusion-based printing	CM: 17.7 ± 2.0 kPa *In vivo* interface adhesion strength: 6.6 ± 1.7 kPa (Day 1), 24.4 ± 6.5 kPa (Day 42)	N/A	[45]
Top: MeHA + diclofenac sodium Cartilage: MeHA + BMSCs/PCL + KGN Osseous: PCL + β-TCP	Composite biochemical (KGN)	BMSCs	Layer-by-layer alternate bioprinting	EM: 85 ± 10 MPa (cartilage), 185 ± 15 MPa (osseous) S: 55 ± 5 N/mm (cartilage), 110 ± 8 N/mm (osseous) Maximum stress: 1.5 ± 0.1 MPa (cartilage), 3.0 ± 0.2 MPa (osseous)	Rat	[46]
Cartilage: GelMA Osseous: GelMA-HAp (1% w/t)	Composite	Cell-free	Continuous 3D printing	CM: 300 ± 50 kPa (cartilage), 500 ± 70 kPa (osseous)	Rabbit	[47]
Cartilage: PLGA + fibrin Intermediate: PLCL + CS/BG Osseous: Calcium silicate ceramic	Composite biochemical	BMSCs	Electrospinning + extrusion-based printing	CM: 0.54 ± 0.04 MPa (cartilage), 33.6MPa (osseous) YM: 5.1 ± 0.8 MPa (intermediate)	Rabbit Minipig	[48]
Cartilage: SF Osseous: PEGT/PBT mesh+ porous silk	Composite	Cell-free	FDM + extrusion-based printing	CM: 0.12 ± 0.01 MPa (cartilage), 12.56 ± 1.94 MPa (osseous), 0.113 ± 0.028 MPa (fibrin scaffold)	N/A	[49]
Top: PGS-CS Bottom: Gelatin	Composite	Cell-free	FDM + extrusion-based printing	CM: 0.162 ± 0.005 MPa (PGS, dry); 0.159 ± 0.003 MPa (PGS, wet); 1.139 ± 0.052 MPa (PGS-Gel, dry); 0.195 ± 0.007 MPa (PGS-Gel, wet); 2.443 ± 0.071 MPa (PGS-CS/Gel, dry); 0.315 ± 0.019MPa (PGS-CS/Gel, wet)	Rabbit	[50]
Cartilage: TPU + Gel-Alg Osseous: PLA + HAp	Composite	Cell-free	FDM + extrusion-based printing	CM: 1.079 ± 0.031 MPa (cartilage), 44.369 ± 2.515 MPa (osseous), 21.336 ± 3.683 MPa (total) Shear strength: 0.73 ± 0.027 N YM: 45 MPa (PLA/HAp), 1 MPa (TPU)	Rabbit	[51]

(Continued....)

Table 2. Continued...

Scaffold design	Strategy	Seed cell	Manufacturing method	Mechanical properties	*In vivo* model	Reference
Cartilage: SF Osseous: PEGT/PBT mesh + porous silk	Biochemical (TGF-β1 binding)	Cell-free	UV crosslinking + peptide grafting	CM: 120 kPa (GelMA) TGF-β1 binding peptides reduce the CM.	Rat	[52]
Upper: PGS-CS Bottom: Gelatin	Biochemical (dECM + exosome)	Cell-free	Extrusion-based printing	Reduced modulus: 6.3 ± 0.4 MPa (bilayer hydrogel-exosome), 5.7 ± 0.3 MPa (bilayer hydrogel)	Rat	[53]
Cartilage: TPU + Gel-Alg Osseous: PLA + HAp	Biochemical (thiolated heparin / strontium nanoparticle)	eUCB-MSC	High-throughput microfluidics-based fabrication	CM: approximately 2 MPa of PEGT-PBT scaffold	N/A	[54]
Cartilage: GelMA + KGN (high concentration) Osseous: GelMA + KGN (low concentration)	Biochemical (KGN)	Cell-free	Sequential bioprinting	CM: 190 ± 15 kPa (cartilage), 210 ± 20 kPa (osseous). Interfacial shear strength: 40 kPa.	Rat	[55]
Cartilage: GelMA + DCM Osseous: GelMA + DBM	Biochemical (dECM)	Murine osteoblast/ chondrogenic cell precursors	DLP	CM increased with the incorporation of dECM (data not specified)	N/A	[56]
Cartilage: GelMA + BP + hUMSCs exosome Osseous: GelMA + BP + hUMSCs exosome + β-TCP	Biochemical (phosphate)	Cell-free	Extrusion-based printing	CM: 48.99 ± 15.67 kPa (3% β-TCP-GelMA). YM: 232.86 ± 12.45 kPa (1% β-TCP), 306.17 ± 17.82 kPa (3% β-TCP)	Rabbit	[57]
Cartilage: PEGDA (1MPa) Osseous: PEGDA (7MPa),	Structural (geometry/ porosity)	Cell-free	SLA/ DLP	S: 1 MPa (cartilage), 7 MPa (osseous) Porosity: cartilage 81% (cartilage), 68% (osseous) CM: 11.8 MPa	N/A	[58]
Bi-phasic: Infill density 45% and 60% Tri-phasic: Infill density 30%, 45% and 60% Gradient: Infill density from 30% to 60%; smooth transition in 7 layers	Structural (infill density)	C28/I2 hChon	Concurrent printing + FDM	CM 397.24 ± 41.51 MPa (bi-phasic, 45%); 213.75 ± 32.17 MPa (bi-phasic, 60%); 397.24 ± 41.51 MPa (bi-phasic, total); 228.98 ± 40.84 MPa (tri-phasic, 30%); 140.56 ± 21.73 MPa (tri-phasic, 45%); 118.99 ± 29.13 MPa (tri-phasic, 60%); 228.98 ± 40.84 MPa (tri-phasic, total). Gradient:177.98 ± 44.78 MPa (total)	N/A	[59]
4 layers PCL scaffold with different pore sizes infilled with cell-laden hydrogel	Structural (pore size)	BMSCs	FDM	Pore size of four layers: 150, 350, 550, and 750 μm	Rabbit	[60]

(Continued....)

Table 2. Continued...

Scaffold design	Strategy	Seed cell	Manufacturing method	Mechanical properties	*In vivo* model	Reference
Cartilage: GelMA (lotus/radial pores) + KGN Osseous: GelMA (lotus pores)	Structural (geometry) + biochemical (KGN)	Cell-free	DLP	CM: 388.0 ± 17.52 kPa (15% GelMA, 0 μm porosity); 344.3 ± 16.50 kPa (15% GelMA, 100 μm porosity); 302.0 ± 15.00 kPa (15% GelMA, 200 μm porosity); 203.3 ± 10.41 kPa (15% GelMA, 400 μm porosity); 178.0 ± 7.211 kPa (10% GelMA, 0 μm porosity); 157.3 ± 6.429 kPa (10% GelMA, 100 μm porosity); 139.0 ± 5.568 kPa (10% GelMA, 200 μm porosity); 107.3 ± 3.055 kPa (10% GelMA, 400 μm porosity)	Rabbit	[61]
Cartilage: hChon + Alg-MC + TGF-β3 Osseous: hOB + Alg-MC + BMP-2	Cell heterogeneity + biochemical	hChon, hOB	Extrusion-based printing	N/A	N/A	[62]
Cartilage: ACPCs + GelMA/AlgMA Osseous: BMSCs + GelMA/AlgMA	Cell heterogeneity + biochemical	ACPCs, BMSCs	Extrusion-based printing	YM: ~ 15 kPa.	Rabbit	[63]
Cartilage: PCL/gelatin/fibrin Osseous: PCL/HA nanoparticles	Composite	Cell-free	Extrusion-based printing	Compressive strength: 2.1 MPa (10% fibrin), 0.81 MPa (30% fibrin)	N/A	[64]

Abbreviations: ACPCs, articular cartilage progenitor cells; Alg, alginate; AlgMA, methacrylated alginate; BG, bioactive glass; BMP2, bone morphogenetic protein-2; BMSCs: bone marrow-derived mesenchymal stem cells; CM, compressive modulus; CS, chondroitin sulfate; DBM, decellularized bone matrix; DCM, decellularized cartilage matrix; DLP, digital light processing; dECM, decellularized extracellular matrix; EM, elastic modulus; eUCB-MSC, expanded umbilical cord blood-derived mesenchymal stem cells; FDM, fused deposition modeling; GelMA, gelatin methacrylate; HAp, hydroxyapatite; hChon, human chondrocytes; hOB, human osteoblasts; KGN, Kartogenin; MC, methylcellulose; MEW, melt electrowriting; MeHA, methacrylated hyaluronic acid; PCL, polycaprolactone; PCaP, polymer calcium phosphate; PEGDA, polyethylene glycol diacrylate; PEGT/PBT, poly(ethylene glycol)-terephthalate/poly(butylene terephthalate); PGS, poly(glycerol sebacate); PLA, polylactic acid; PLCL, poly(L-lactide-co-caprolactone); PLGA, poly(lactic-co-glycolic acid); S, stiffness; SA, sodium alginate; SF, silk fibroin; SLA, stereolithography; TCP, tricalcium phosphate; TGF, transforming growth factor; TPU, thermoplastic polyurethane; YM, Young's modulus.

a polyelectrolyte multilayer (PEM) system, which was coated with dexamethasone-loaded liposomes. The study demonstrated that the involvement of dexamethasone-loaded liposomes exhibited more prominent chondrogenic differentiation compared to the baseline PEM system.

Gene therapy offers a promising strategy for osteochondral regeneration by delivering genes essential for cartilage and bone repair or silencing pathological genes associated with joint disease, creating a gene expression gradient to achieve zonal cell differentiation.[104] Commonly used genes include growth factors such as IGF-1,[105] TGF-β,[106,107] BMP,[21] and FGF; transcription factors such as SOX9; and anti-inflammatory molecules like interleukin (IL)-10[108] and IL-1 receptor antagonist (IL-1RA).[109] Traditional gene delivery often relies on viral vectors.[110] Despite their efficiency, viral vectors face limitations, including pre-existing immunity to viruses like adenovirus, which reduces their effectiveness. Additionally, the limited duration of transgene expression, lasting approximately only 1–2 weeks, hinders long-term use *in vivo*.[110] Therefore, non-viral vectors, such as nanoparticle carriers and mRNA delivery, are gaining attention as promising alternatives.

MicroRNAs (miRNAs) have introduced a novel approach to gene therapy due to their ability to precisely regulate the spatial and temporal expression of target genes and associated pathways, which are crucial for chondrogenesis and cartilage development.[111] Notably, reduced levels of miR140-5p have been observed in progenitor/stem cells (CPCs) from OA cartilage, indicating a correlation with OA progression.[112] Exosomes, with low immunogenicity, targeted delivery, and excellent biocompatibility, could serve as a promising carrier for miRNA delivery in gene therapy.[113] Nanoparticles, featuring a porous organosilicon structure, efficiently encapsulate and deliver miRNA with temporal release. Zhu et al.[114] developed a self-healing hydrogel loaded with

Mesoporous organosilicon-Polyethyleneimine (MON-PEI) nanoparticles for stable miRNA140-5p transfection, showing effective cartilage defect repair in a rabbit joint model.

3.4. Cells heterogeneity

Cell-laden hydrogel 3D printing has gradually drawn attention in the last decade. Cells employed for osteochondral regeneration include MSCs, such as BMSCs and adipose-derived stem cells (ADSCs), articular cartilage progenitor cells (ACPCs), and induced pluripotent stem cells (iPSCs).[115] MSCs show low immunogenicity and good *in vivo* safety, becoming the most widely used cell in regenerative medicine.[116] Although technically pluripotent, MSCs rarely repair damaged tissue *in vivo* through direct differentiation and engraftment due to certain limitations, including the reduced capacity of these cells for self-renewal, proliferation, and differentiation in donor sites.[117] Besides, BMSCs are inclined to differentiate into bone tissue rather than cartilage.[118,119] Therefore, scaffolds require the modulation of differentiation through cytokines or drugs. However, the side effects associated with cytokines, combined with their high costs, present significant limitations for their clinical use *in vivo*. For example, although TGF-β is proven to induce chondral differentiation, Zhen et al.[120] reported that overactivation of the TGF-β1 pathway in subchondral bone may lead to pathological changes associated with cartilage degeneration. Furthermore, the release kinetics and half-life of small molecules *in vivo* restrict their long-term therapeutic efficacy.[121] Therefore, a bicellular scaffold could be a promising approach for tissue regeneration. Bicellular scaffolds enable precise spatial cell alignment by delivering the cells during the printing process, rather than relying on intrinsic cell migration. Furthermore, the bicellular system enhances tissue function and structural reconstruction through cell–cell interactions, enabling the synchronous repair of different tissues.[63]

Möller et al. demonstrated that co-encapsulation of hBMSCs and human nasoseptal chondrocytes (hNCs) within GelMA hydrogels for 3D bioprinting resulted in more pronounced ECM deposition compared to hBMSCs alone.[122] Wu et al.[123] developed a bicellular 3D-printed liver lobule-mimetic structure, demonstrating that the HepG2 + NIH/3T3 bicellular system enhanced HepG2 proliferation and function compared to monocellular systems, which can be attributed to crosstalk pathways via NIH/3T3-secreted cytokines and growth factors. The bicellular model better mimics the physiological microenvironment, improving cell–cell/matrix interactions and enhancing functionality.

Zhang et al. developed a bicellular anisotropic hydrogel scaffold using 3D printing. ACPCs were incorporated into the upper hydrogel layer to simulate cartilage, while BMSCs were placed in the lower layer for bone regeneration. The 3D printing technique enabled precise, layer-specific placement of cells, facilitating independent functionality and spatial alignment of cartilage and bone. ACPCs and BMSCs promote cartilage and bone formation through the secretion of specific growth factors and ECM components. Cell–cell interactions simultaneously stabilize the cartilage–bone interface, with BMSCs in the osseous layer driving both bone matrix production and angiogenesis, thus enhancing nutrient supply. Vascular penetration into the cartilage layer is suppressed by the cartilage matrix secreted by ACPCs, maintaining low vascularization within the cartilage.

4. Pivotal properties of scaffolds for *in vivo* application

4.1. Degradation rate

During osteochondral repair, scaffolds must provide temporary and adequate mechanical support to the defect site while degrading at a controlled rate to allow regenerated tissue to replace the scaffold and integrate with surrounding tissue. *In vivo*, osteochondral regeneration typically progresses through the following stages[123]: (1) the inflammatory stage, where immune cells remove dead cells from the damaged tissue to establish a foundation for regeneration; (2) the proliferating stage, lasting approximately 2–6 months, during which endogenous cells migrate to the injury site as the scaffold degrades, proliferate, differentiate, and gradually replace the scaffold; and (3) the remodeling stage, during which the biophysical properties of the newly formed tissue further enhance and replace the scaffold to become the predominant load-bearing component. This stage could last several months. Throughout the process, the biophysical properties of the newly formed tissue improve as the scaffold's mechanical support diminishes, establishing a dynamic balance that preserves the mechanical stability of the osteochondral tissue.[124] Therefore, the degradation kinetics of scaffolds must synchronize with tissue growth.[125] Meanwhile, since bone has higher mechanical support requirements than cartilage, the degradation rate of bone-phase scaffolds is typically slower than that of cartilage-phase. *In vitro* studies reveal that the cartilage phase degrades almost completely within approximately 12 weeks, aligning with cartilage regeneration, while bone-phase scaffolds require a longer degradation period, typically 16–24 weeks or more.[47,48,54]

The degradation rate of scaffolds is influenced by multiple aspects, including chemical composition, geometric structure, porosity, and microenvironment. Blending two or more polymer materials is a common

way to regulate the degradation kinetics. For instance, incorporating HAp[54] and β-TCP nanoparticles[55] into GelMA hydrogels can reduce the degradation rate for bone-phase scaffolds. Gao et al.[54] improved the degradation performance of GelMA scaffolds by adding 1% HAp. *In vitro,* phosphate-buffered saline (PBS) degradation tests showed that scaffolds without HAp exhibited more than 70% weight loss after 4 weeks, while those with HAp degraded by only 50%. dECM can also retard the degradation rate. Li et al.[53] evaluated the residual mass percentage and revealed a significant reduction in the degradation rate with the addition of dECM. Bejarano et al.[126] reported that incorporating BG into the poly(D, L-lactic acid) (PDLLA) polymer could accelerate the degradation rate while simultaneously maintaining the scaffold's dimensional and structural integrity.

Degradation kinetics of scaffolds are influenced by their mesostructure, including factors such as porosity, pore size, pore shape, grain size, and crystallinity. A higher porosity generally leads to an increased degradation rate,[127] as scaffolds with more micropores and a larger surface area facilitate the diffusion of degradation products, thereby accelerating the process. Larger pores also allow better penetration of degradation products and moisture, promoting cell growth and tissue infiltration, which further speeds up degradation.[127,128] Conversely, smaller grain sizes reduce the degradation rate because they increase the grain boundary area, hindering the diffusion of degradation products and enhancing the material's strength.[129]

The inflammatory microenvironment, including cytokines and enzymes, can significantly influence the degradation rate. In the microenvironment of OA, a wide range of enzymes and cytokines undergo significant alterations. Notably, MMP families, which are capable of cleaving collagen type II, play a pivotal role in cartilage degradation.[130] Liu et al.[46] established a triple-layer scaffold consisting of BMSC-laden methacrylated HA (MeHA), PCL, and KGN as the chondral layer, coated with a MeHA plus diclofenac sodium layer, and a PCL plus β-TCP osseous layer. MeHA, a rapidly degradable material, has a tunable degradation rate influenced by enzymes such as MMPs. MMP-sensitive MeHA allows for the modulation of degradation rate and surface drug release in response to disease activity, such as inflammation in arthritis.

To estimate the degradation rate, weight loss is a standard approach for *in vitro* studies, where scaffolds are incubated in simulated body fluid or PBS for 12 weeks, and the remaining mass is measured periodically.[42,48,54,55] *In vivo*, histological evaluation is commonly employed to monitor scaffold degradation and tissue formation at the defect site, providing insights into the material's biological performance over time.[47]

4.2. Interlaminar interface strength

In *in vivo* studies, mechanical stability is considered a critical factor for successful regeneration. Beyond the intrinsic mechanical properties of scaffolds, interface strength—another crucial element—plays a pivotal role in ensuring the efficacy of the repair process. This encompasses two key aspects: the strength of the interlaminar interface (horizontal integration),[131] and integration with native tissue (lateral integration).[132]

During scaffold-based regeneration of osteochondral defects, the interface between the cartilage and bone phases is prone to stress concentration due to the discontinuity in their mechanical properties.[133] Therefore, tissue engineering scaffolds need to achieve an effective integration between cartilage and bone tissue.

However, bilayered or multilayered scaffolds are often ineffective in biomimicking osteochondral tissue due to the potential for delamination between layers.[134] Current strategies for enhancing interlaminar interface strength can be broadly categorized into the following approaches: (1) interlamellar bonding, (2) mechanical interlocking through contact surface topography design, (3) tissue culture with cell seeding, and (4) specified 3D printing techniques.

Bonding is a traditional method to integrate two layers, which can be achieved through chemical bonding or solvent bonding. The dual-phase interface can be modified by introducing reactive group-containing agents that form chemical bonds between components and the biopolymer matrix through chemical interactions. Coyle et al.[56] developed a bilayer dECM-incorporated GelMA scaffold, in which the double layers were chemically bonded using 1-ethyl-3-(3-dimethylaminopropyl) carbodiimide/ N-hydroxysuccinimide (EDC/NHS) coupling. EDC activates the carboxyl groups on the GelMA hydrogels, generating highly reactive O-acylisourea intermediates, which are stabilized by NHS. These intermediates then react with primary amines on the second hydrogel layer, forming amide bonds and effectively conjugating the layers. This method ensures strong covalent bonding, enhancing the structural integrity and interface compatibility of the composite material.

Liuyun et al.[135] designed a method for modifying nano-HAp with the assistance of L-lysine, and incorporated the modified HAp into poly(lactic-co-glycolic acid) (PLGA) to fabricate nanocomposites. L-lysine bonds to the HAp surface through the formation of a calcium-carboxylate linkage between the calcium of HAp and

the carboxylate group of L-lysine, thereby improving the interface compatibility between the HAp particles and the PLGA matrix.

Interlocking is a mechanical bonding method where material surfaces engage through geometric features such as grooves, hooks, or ridges, thereby enhancing adhesion and structural integrity without the need for adhesives or chemical bonding. 3D printing, as a high-precision manufacturing technique, is ideal for creating interlocking surfaces. When utilizing FDM or stereolithography (SLA) to print materials with varying properties, interlocking designs can be incorporated to strengthen the interlayer adhesion.[43] According to the review by Nedrelow et al.[136] focusing on scaffold interface design, interlocking a robust 3D-printed bone phase with a cartilage phase hydrogel is the most effective method for enhancing the interface strength. Diloksumpan et al.[45] created a bilayer scaffold with an interlocking interface design. The bone phase consisted of a bone-biomimetic ceramic ink containing tricalcium phosphate, nanohydroxyapatite, and a custom-synthesized biodegradable poloxamer, while the cartilage phase was composed of MEW-printed PCL microfibers and gelatin-based hydrogel loaded with chondroprogenitor cells. During printing, the PCL microfibers interlaced with the ceramic matrix, protruding into the cartilage region. This spatially organized arrangement enabled mechanical interlocking between the bone and cartilage phases. Compared to non-interlocking designs, the adhesion strength between the composite hydrogel and ceramic increased by over 6.5 times. The fiber within the ceramic scaffold enables more effective lateral constraint of the hydrogel under axial compression, resulting in a stronger mechanical response.

Although interface strength can be enhanced through bonding strategies, it remains inferior to that of native mature bone-cartilage boundaries.[137] Hence, using cell-laden materials to induce *in situ* regeneration at the defect site may offer a promising solution. Current scaffold designs still suffer from uneven cell distribution. The inability to precisely control cell placement and spatial alignment often results in discrepancies in cell density, potentially compromising the efficacy of tissue repair.[138] ECM secretion by cells may help to create a more harmonious interface. Wang et al.[139] designed a cell-based strategy to improve integration and transition between cartilage and osseous layers by sandwiching a human umbilical cord mesenchymal stem cells (hUCMSCs) layer between the constructs before suturing. Histological and immunohistochemical analyses showed more uniform ECM distribution in the cell-loaded constructs, while the control group exhibited V-shaped gaps at the interface due to a lack of cells and ECM.

Co-printing involves the simultaneous or sequential deposition of different materials within a single 3D printing process, enabling the creation of complex, functional structures, and interfaces. This requires 3D printers with multiple print heads, each capable of handling distinct materials.[136] Continuous 3D printing provides another approach to enhance the mechanical properties.[140] In continuous 3D printing, the print head deposits successive material layers without interruption, ensuring seamless integration and smooth transitions between materials. This method effectively eliminates the interface misalignment or gaps often seen in traditional layer-by-layer printing.[47]

4.3. Scaffold-native tissue integration

The mechanical discontinuity at the scaffold-native tissue interface significantly hinders integration. Yodmuang et al.[141] that interface strength before mechanical loading and shear stresses within the scaffold during loading are key determinants of integration. Periodic axial forces of 1 and 6 N were applied to the scaffold to simulate the contact stress experienced by cartilage during daily activities and their effects on scaffold–cartilage interface integration were evaluated. The results indicated that 1 N loading resulted in poor integration between the scaffold and cartilage, whereas 6 N loading significantly enhanced interface strength, demonstrating that higher loading intensity more effectively promotes integration. This effect may be attributed to increased shear and interface stresses, which facilitate scaffold–cartilage cell adhesion and accelerate cell and matrix migration and proliferation. Moreover, high-intensity loading improves mechanical matching between the scaffold and cartilage; simulates physiological loading; and enhances cartilage cell migration, ECM synthesis, and cross-linking. It also activates cellular mechanosensing pathways, promoting cell proliferation, differentiation, and exosome secretion. However, the detailed mechanisms are not yet illustrated; hence, studies devoid of mechanical analysis may lack translational relevance for clinical applications.

Crosslinking of ECM between the scaffold and native tissue can enhance integration. Zhao et al.[142] present a multifunctional scaffold loaded with lysyl oxidase (LOX) plasmid DNA, exosomes, and manganese dioxide nanoparticles (MnO_2 NPs). LOX facilitates ECM crosslinking, strengthening the mechanical bonding between the scaffold and tissue. Concurrently, MnO_2 NPs efficiently scavenge excess ROS at the injury site, preventing ECM degradation and thereby potentiating the crosslinking activity of LOX.

Cell-laden scaffolds offer a promising way to enhance scaffold–tissue integration. Claramunt et al.[143] developed a polyurethane meniscal scaffold coated with fibronectin. The

quality of the newly formed meniscal tissue was assessed *in vivo* by the rabbit model. Compared to scaffolds without MSC loading, the incorporation of MSCs into the scaffold significantly improved scaffold integration, proteoglycan synthesis, and the mechanical properties of the newly formed tissue. Similarly, Chung et al.[144] demonstrated that hUCMSCs-laden 4% HA hydrogel significantly enhanced cartilage quality histologically, achieving a remarkable collagen pattern and cell arrangement that closely resemble the structure of adjacent native cartilage.

4.4. Evaluation assays for interface strength

The interlaminar interface strength can be evaluated mechanically or histologically. For example, in the interface shear test, the osseous phase is fixed while a lateral force is applied to the chondral phase.[36] In contrast, the lap shear test relies on sandwiching the bilayer scaffold between two tabs, with both surfaces of the scaffold being stuck to the tabs with adhesive. The laps are then subjected to tensile loading in opposite directions.[145] Additionally, interface strength can be evaluated using the peel test, in which the chondral phase is gripped and a force perpendicular to the interface is applied to induce delamination from the osteal phase.[146] Compared to the interface shear test, the lap shear test requires extra clamping or adhesive bonding of the scaffold, which may introduce additional artifacts in evaluation.[36] While the peel test provides insight into interface strength, its loading condition failed to replicate *in vivo* scenarios. Given these considerations, the interface shear test is generally regarded as the most appropriate method for evaluating interface strength.[136] Additionally, histological studies can reveal the tissue growth pattern, including cell density, cell alignment, and ECM, which can serve as an important reference for assessing interface integration.[139]

The integration efficacy between the scaffold and native tissue can be quantitatively assessed through mechanical evaluation. Specifically, the push-out test serves as a standardized assay to determine interfacial adhesion strength, in which an axial compressive load is applied parallel to the scaffold–tissue interface until interfacial failure occurs. The maximum load at failure is recorded and normalized to the total surface area of the scaffold's luminal interface, enabling the calculation of the ultimate interfacial shear strength.[141] This parameter provides a quantitative measure of the biomechanical integrity at the scaffold–tissue interface (Figure 4).

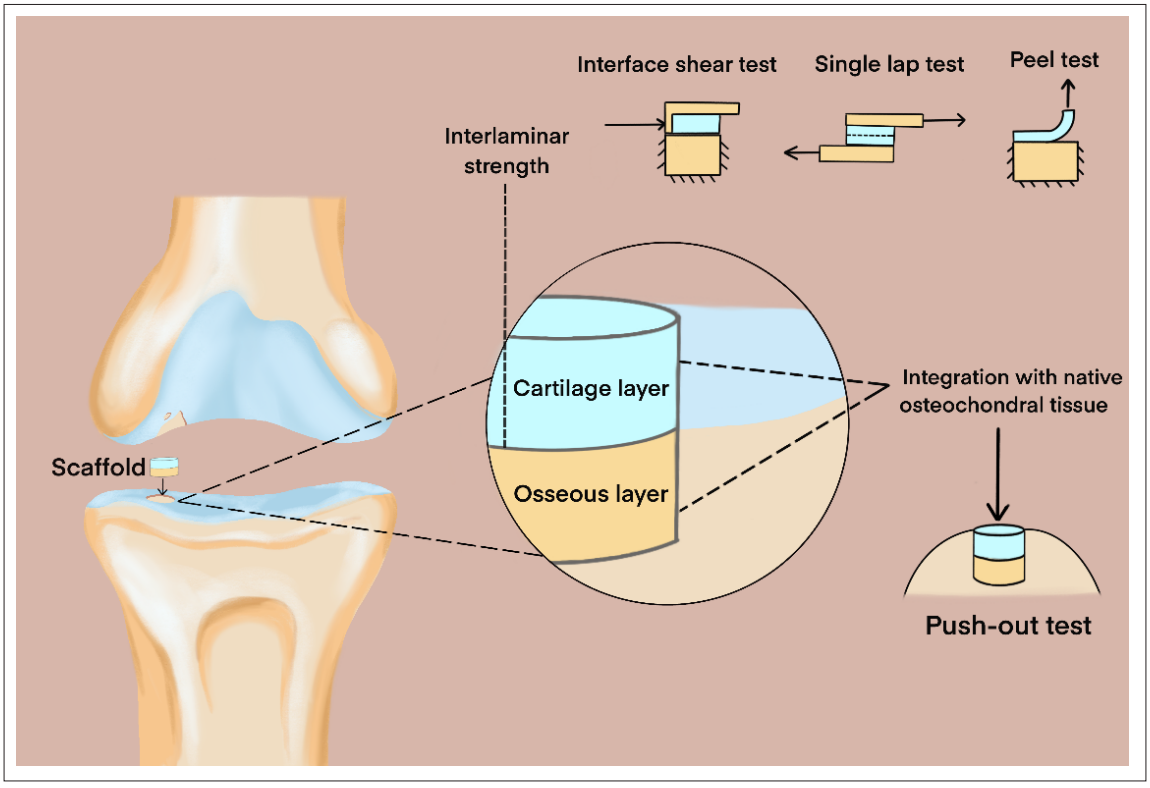

Figure 4. Evaluation assays for interlaminar and integration strength for bilayer scaffold.

5. Discussion

5.1. 3D printing methodology

With the development of bioprinting methods and ink materials compatible with bone engineering, various 3D printing techniques have been applied to fabricate osteochondral scaffolds. Conventional 3D printing, such as SLA, FDM, and selective laser sintering (SLS), involves layer-by-layer deposition of materials. In contrast, 3D bioprinting creates 3D artificial implants or complex tissues through layer-by-layer deposition of living cells, ECM, and other biomaterials. Common techniques for bioprinting include inkjet-based bioprinting, extrusion-based bioprinting, and laser-assisted bioprinting.[147]

As shown in the studies of hierarchical printed scaffolds in Table 2, scaffolds employing different strategies tend to adopt specific 3D printing technologies. Extrusion-based printing is the most commonly used method across all strategies. Extrusion-based bioprinting is compatible with a wide variety of materials and does not involve a heating process, making it particularly suitable for printing materials with high cell densities and biological activity.[147,148] Due to nozzle size limitations, extrusion- and inkjet-based 3D printing can only produce microstructures at a minimum scale of 100 μm.[58] However, the fine strain within the cartilage changes at a length scale ranging from 10 to 100 μm.[149,150]

In contrast, scaffolds designed with a microarchitectural gradient strategy tend to apply SLA and DLP,[60,61,58,59] as these printing methods offer higher resolution and can create finely detailed microstructures.[151,152] In particular, microstereolithography (μSLA) enables layer-by-layer fabrication of high-resolution constructs with spatially programmable mechanical properties. By precisely regulating exposure parameters (e.g., duration, light intensity), this technique achieves *z*-axis control over both microstructure and compressive modulus at 10–50 μm resolution.[58,153] Such precision facilitates the development of biomimetic osteochondral scaffolds replicating native tissue's hierarchical mechanical gradients. The characteristics of various printing technologies are summarized in Table 3.

In addition to manufacturing the structure of the scaffold itself, creating fine micro-structures at the interlayer interfaces using high-precision 3D printing techniques also positively impacts the interfacial bonding strength. **Section 4.2** discusses methods to enhance interface strength through interlocking design. The interlocking features created by high-resolution methods,

Table 3. Comparison of 3D printing technologies for osteochondral scaffold design

Technology	Advantages	Disadvantages	Materials
Inkjet-based printing[147,154,155]	Low cost High cell viability High throughput	Limited resolution Non-continuous printing Nozzle clogging Heat damage to cells	Low-viscosity biomaterials (<20 mPa·s)
Extrusion-based printing[62,148,150,156]	Broad range of bioink selection Short fabrication time High cell density and ≠viability	Limited resolution Shear stress damage to cells	Compatible with a wide range of materials
Laser-based printing[157]	High resolution High cell viability and density Nozzle-free	High cost Long fabrication time Relatively low 3D built-up capability	Photocurable resins/nanocomposites Wide range of viscosities
SLA[158,159]	High resolution Layer thickness adjustable Smooth surface finish	Limited materials High cost Post-processing required	Resins only
FDM[73,151,160,161]	Quick fabrication Low-cost Strong layer bonding	Limited materials Limited resolution	Molten thermoplastic material only
DLP[61,162]	High resolution	Limited materials Slow fabrication	Photopolymers
MEW[45,155]	Ultra-fine fiber production Precise porosity control	Limited materials High cost Slow fabrication	Thermoplastic conductive polymers

Abbreviations: DLP, digital light processing; FDM, fused deposition modeling; MEW, melt electrospinning writing; SLA, stereolithography.

such as MEW,[45,163] enhance the structural stability during both the processing and implantation stages.[145]

5.2. Cell-free versus cell-laden strategies

Over the past decade, notable progress has been achieved in cell-free scaffold-mediated *in situ* osteochondral regeneration. However, critical unresolved challenges persist, including: (1) structural incompatibility between scaffolds and defect topography, (2) inadequate recruitment of endogenous host cells, and (3) suboptimal remodeling of neo-formed tissues.[164] The limited diffusion capacity of oxygen and nutrients within conventional scaffolds, compounded by progressive peripheral mineralization, establishes a diffusion barrier that restricts cellular infiltration to superficial regions.[165] This results in preferential survival of cells localized near the scaffold surface, while deeper regions remain sparsely populated. Bioprinting with cell-laden materials offers a promising alternative by enabling precise spatial deposition of pre-seeded cells within scaffolds. However, a fundamental limitation persists in maintaining the long-term viability and functional persistence of encapsulated cells, particularly under sustained physiological stresses.[166]

Ongoing research should focus on biomaterial optimization to achieve biomimetic cell alignment, density, and ECM patterns to better resemble native tissue.

5.3. Vasculature in osteochondral regeneration

During *in vivo* osteochondral regeneration, angiogenesis serves as a prerequisite for osteogenesis, as neo-vasculature provides indispensable metabolic support for bone-forming cells.[167] Inadequate vascularization results in hypoxic microenvironments and cellular necrosis. Oxygen diffusion constraints restrict metabolically active osteoblasts/osteocytes to within 100–200 μm of functional capillaries to sustain viability and biosynthetic activity.[168] Cartilage, however, must preserve avascularity to avoid pathological ossification and complications, necessitating precise spatial regulation of vascularization in scaffold-based osteochondral regeneration. Current approaches focus on dual-pathway control: pro-angiogenic growth factors such as VEGF and bFGF[169,170] are selectively incorporated into subchondral regions to stimulate vascular infiltration, while anti-angiogenic compounds (e.g., suramin and bevacizumab)[171,172] are embedded within cartilaginous zones to inhibit ectopic vessel formation. Besides this biochemical strategy, a physical barrier—typically a semipermeable membrane engineered to block endothelial cell migration while permitting metabolic exchange—is interposed between osteochondral layers to anatomically restrict vascular encroachment into cartilage layers.[167]

Cell-laden scaffolds can demonstrate dual angiogenic modulation through both direct angiogenic differentiation and paracrine signaling mechanisms. Qin et al.[173] established a pre-vascularized scaffold by encapsulating human umbilical vein endothelial cells (HUVECs) within Li-Mg-Si (LMS) ceramic-incorporated GelMA scaffolds. This design significantly enhanced angiogenic functionality, evidenced by robust neovascularization through both HUVEC-derived capillary network formation and amplified VEGF secretion. Notably, the endothelial paracrine profile concurrently stimulated neurogenic precursor proliferation and bone marrow stromal cell osteogenic differentiation, thereby establishing a multifunctional regenerative microenvironment.

Cellular regulation of angiogenesis demonstrates zonal specificity in osteochondral regeneration. Zhang et al.[63] engineered an anisotropic bilayer scaffold by spatially embedding ACPCs in chondral layers and BMSCs in osseous layers. During regeneration, ACPCs maintained avascularity through paracrine secretion of anti-angiogenic factors (e.g., endostatin, chondromodulin-1) and transcriptional downregulation of pro-angiogenic factors (e.g., VEGF, EGF). Meanwhile, osteogenic-phase BMSCs promoted vascular invasion via sustained release of angiogenic signals (e.g., ANGPT1, VEGFA, endomucin), which stimulated endothelial cell proliferation, chemotaxis, and lumenogenesis through ERK1/2-MMP9 pathway activation. Similarly, Liang et al.[174] engineered GelMA-alginate core-shell microcapsules for dual encapsulation of human dental pulp stem cells (hDPSCs) and HUVECs. Compared to monoculture groups containing either hDPSCs or HUVECs alone, co-cultured groups exhibited elevated proliferation rates. Notably, 3D capillary-like networks formed in all hDPSC-containing co-culture microcapsules, regardless of cell ratio, with significant increases vasculogenesis markers after 14 days of culture (e.g., percentage vascular area, branch length, branch number, and junction points). In contrast, hDPSC-deficient groups showed no vasculogenesis at day 14, demonstrating the essential role of intercellular interactions during vascularization. Given the persistent challenge of vascularizing osteochondral interfaces, scaffolds designed with a cell heterogeneity strategy offer a promising way to address this critical limitation in tissue engineering.

5.4. Inflammatory microenvironment *in vivo*

Osteochondral defects are often accompanied by inflammatory alterations in the local microenvironment. The persistent presence of an inflammatory environment is a major obstacle to cartilage repair, as it may limit the recruitment of endogenous cells to the site, ultimately leading to the failure of *in situ* cartilage regeneration.[175]

Therefore, improving the inflammatory microenvironment at an early stage should be prioritized to achieve better repair outcomes. The alleviation or deterioration of inflammatory markers can reflect the repair status, including the following: (1) pro-inflammatory cytokines, such as IL-1β, IL-6, IL-8, and tumor necrosis factor-alpha (TNF-α); (2) macrophage polarization (M2/M1 ratio) assessed by flow cytometry[176]; (3) immune cell infiltration (e.g., T lymphocytes, neutrophils) assessed by immunostaining[43]; and (4) oxidative stress levels, such as reactive oxygen species (ROS),[177] lipid peroxidation products (e.g., malonaldehyde),[178] and antioxidant enzyme activities (e.g., superoxide dismutase, catalase).[179]

As an implanted foreign material, the inflammatory response induced by scaffolds should be considered. Most studies reviewed in this article did not focus on inflammation-related responses. Nedrelow et al.[43] observed CD4+ T cell infiltration following scaffold implantation; however, this does not necessarily indicate the level of inflammation.[180] Li et al.[86] quantitatively analyzed IL-1β levels after implantation, finding a significant increase in the early stage (1 week), which gradually decreased after 4 weeks, suggesting that scaffold implantation induces a mild inflammatory response during the early phase.

The balance between anti-inflammatory and pro-inflammatory pathways within the microenvironment is closely associated with macrophage phenotypes. M1 phenotype generates ROS and inflammatory cytokines.[181,182] ROS directly degrades the chondral ECM, inducing lipid peroxidation and DNA fragmentation, thereby imposing significant limitations and challenges for scaffold-based tissue regeneration.[183] Hence, the concept of ROS-scavenging hydrogels has been proposed to enhance the efficacy of scaffold-based tissue regeneration. Current strategies for ROS scavenging include: (1) anti-inflammatory small-molecule drugs,[175] such as NSAIDs; (2) integration of antioxidant nanoparticles[184]; (3) incorporation of antioxidant enzymes (e.g., catalase) or nano enzymes[184,185]; and (4) fabrication of scaffolds using bioactive materials with inherent antioxidant properties.[186–189]

Liu et al.[183] incorporated cerium oxide nanoparticles functionalized with cerium bifunctional albumin (CeNPs) into GelMA, which counteracted the toxic effects induced by hydrogen peroxide. 2′,7′-dichlorofluorescein diacetate (DCFH-DA) and dihydroethidium (DHE) staining confirmed a reduction in ROS. Furthermore, the scaffold promoted the activation of the PI3K/Akt/EBV1 pathway, facilitating the polarization of gliogenic cells toward the anti-inflammatory M2 phenotype. Deng et al.[190] utilized human hair-derived antioxidant nanoparticles (HNPs) and microparticles (HMPs). These bioactive nanoparticles protected chondrocytes from oxidative stress-induced damage by scavenging ROS, while simultaneously stimulating the HIF-1α and glucose transporter (GLUT) signaling pathways to promote chondrocyte proliferation and maturation.

Combining ROS-scavenging agents with anti-inflammatory drugs demonstrates synergistic efficacy in alleviating inflammatory progression.[191] Lu et al.[192] developed a dual-layer hydrogel system co-loaded with diclofenac sodium and BMSC-derived exosomes. During the early phase, the ROS-responsive upper layer degrades and releases diclofenac, which rapidly improves the inflammatory microenvironment by suppressing lipoxygenase activity, nuclear factor kappa β (NF-κβ) signaling, and M1 macrophage polarization. Subsequently, the sustained release of exosomes promotes cartilage repair. *In vitro* and *in vivo* analyses confirmed reduced expression of pro-inflammatory M1 markers, inhibition of ECM degradation-related genes, and upregulation of cartilage repair-associated genes.

5.5. *In vivo* animal model verification

Osteochondral repair research utilizes animal models across the following different size categories: small rodents (murine and rat models),[193] intermediate species (rabbits and canines),[42] and large animal models (ovine, caprine, equine, and porcine).[194] Current studies predominantly employ small animal models, particularly rabbits and murines, for *in vivo* experimentation. These models offer practical advantages, including short experimental timelines, low maintenance cost, simplified husbandry, and feasibility for large-scale study.[193]

However, there are notable differences between small animals, large animals, and humans, in terms of joint size, load-bearing capacity, anatomical features, and tissue repair potential, which limits the translational relevance of small animal models. For example, human articular cartilage is typically 2–4 mm thick, whereas rabbit cartilage is only 0.25–0.75 mm,[195] and murine cartilage is even thinner. The area of cartilage defects also varies significantly with body size. Strategies effective in small animals may be inadequate to support larger defects, presenting a major challenge. Furthermore, osteochondral defects in rodent models tend to undergo spontaneous repair,[193] which may lead to an overestimation of scaffold efficacy.

Guinea pigs, which exhibit spontaneous cartilage degeneration similar to humans and lack the ability for spontaneous cartilage repair, are widely used as OA models. However, the anatomical features of their knee joints differ significantly from humans and the medial compartment of their knees bears increasing load during movement.[195]

Generally, the knee joints of small animals are in a highly flexed position, unlike in humans.[196] Additionally, humans engage in a wider range of movements—such as walking, squatting, and stair climbing—that generate different mechanical stress patterns on the knee joint compared to animals. Therefore, while experimental success in small animal models is valuable, a gap remains in clinical translation.

In contrast, large animals such as pigs, goats, and horses exhibit biomechanical features and joint sizes that are more similar to humans.[194,197] Validation in these models can provide more clinically relevant data. Nevertheless, significant interspecies differences persist. For example, only the human knee achieves full extension, a feature not observed in common large animal models.[197] Therefore, clinical translation of osteochondral repair strategies requires careful adaptation to human physiological and biomechanical characteristics.

6. Conclusion

Osteochondral defects remain difficult to repair due to the complex structure and specialized function of osteochondral tissue. Recent advances in 3D printing have enabled the fabrication of hierarchical scaffolds that better mimic native tissue and support zone-specific regeneration. This review has highlighted four key strategies—composite gradients, microarchitectural patterning, biochemical gradient, and cellular heterogeneity—as essential approaches to achieving functional hierarchical design. Despite progress, challenges like degradation mismatch, poor interface integration, and inflammatory responses still limit clinical translation. Future research should prioritize the development of stimuli-responsive biomaterials, validation in large-animal models, and the integration of multi-material bioprinting technologies to further advance scaffold-based osteochondral repair.

Acknowledgment

The graphical abstract was created using BioRender.com.

Funding

This work was supported by the Natural Science Foundation of Beijing, China (Grant No. 7232119), the Beijing Natural Science Foundation (Grant No. L232006), Peking Union Medical College Hospital Talent Cultivation Program (Grant No. UHB11847), the National High Level Hospital Clinical Research Funding (No. 2022-PUMCH-C-036), and the National Natural Science Foundation Youth Fund (Grant No. 82102582).

Conflicts of interest

The authors declare no competing interests.

Authors' Contributions

Conceptualization: Qi Wang, Wei Zhu
Writing-Original Draft: Qi Wang
Writing-Review & Editing: Qi Wang, Wei Zhu
I*nvestigation*: Qi Wang, Ruoying Wang
Resources and supervision: Xisheng Weng

Ethics Approval and Consent to Participate

Not applicable

Consent for Publication

Not applicable

Availability of Data

Not applicable

References

1. Mahmoudian A, Lohmander LS, Mobasheri A, Englund M, Luyten FP. Early-stage symptomatic osteoarthritis of the knee - time for action. *Nat Rev Rheumatol*. 2021;17(10):621-632. doi: 10.1038/s41584-021-00673-4

2. He B, Wu JP, Kirk TB, Carrino JA, Xiang C, Xu J. High-resolution measurements of the multilayer ultra-structure of articular cartilage and their translational potential. *Arthritis Res Ther*. 2014;16(2):205. doi: 10.1186/ar4506

3. Soderquist M, Barnes L. Osteochondral allograft transplantation for articular humeral head defect from ballistic trauma. *JSES Rev Rep Tech*. 2024;4(3):540-546. doi: 10.1016/j.xrrt.2024.04.008

4. GBD 2021 Osteoarthritis Collaborators. Global, regional, and national burden of osteoarthritis, 1990-2020 and projections to 2050: a systematic analysis for the Global Burden of Disease Study 2021. *Lancet Rheumatol*. 2023;5(9):e508-e522. doi: 10.1016/s2665-9913(23)00163-7

5. Weng Q, Chen Q, Jiang T, et al. Global burden of early-onset osteoarthritis, 1990-2019: results from the Global Burden of Disease Study 2019. *Ann Rheum Dis*. 2024;83(7):915-925. doi: 10.1136/ard-2023-225324

6. Abdulghani S, Morouço PG. Biofabrication for osteochondral tissue regeneration: bioink printability requirements. *J Mater Sci Mater Med*. 2019;30(2):20. doi: 10.1007/s10856-019-6218-x

7. Brophy RH, Fillingham YA. AAOS clinical practice guideline summary: management of osteoarthritis of the

knee (nonarthroplasty), third edition. *J Am Acad Orthop Surg*. 2022;30(9):e721-e729.
doi: 10.5435/jaaos-d-21-01233

8. Medina J, Garcia-Mansilla I, Fabricant PD, Kremen TJ, Sherman SL, Jones K. Microfracture for the treatment of symptomatic cartilage lesions of the knee: a survey of International Cartilage Regeneration & Joint Preservation Society. *Cartilage*. 2021;13(1_suppl):1148s-1155s.
doi: 10.1177/1947603520954503

9. Patel S, Caldwell JM, Doty SB, et al. Integrating soft and hard tissues via interface tissue engineering. *J Orthop Res*. 2018;36(4):1069-1077.
doi: 10.1002/jor.23810

10. Lee CH, Cook JL, Mendelson A, Moioli EK, Yao H, Mao JJ. Regeneration of the articular surface of the rabbit synovial joint by cell homing: a proof of concept study. *Lancet*. 2010;376(9739):440-448.
doi: 10.1016/s0140-6736(10)60668-x

11. Patel JM, Merriam AR, Culp BM, Gatt CJ, Jr., Dunn MG. One-year outcomes of total meniscus reconstruction using a novel fiber-reinforced scaffold in an ovine model. *Am J Sports Med*. 2016;44(4):898-907.
doi: 10.1177/0363546515624913

12. Ayers DC. How common is revision for adverse reaction to metal debris after total hip replacement with a metal-on-polyethylene bearing surface?: commentary on an article by Anders Persson, MD, et al.: "Revision for Symptomatic Pseudotumor Following Primary Total Hip Arthroplasty with a Standard Femoral Stem". *J Bone Joint Surg Am*. 2018;100(11):e82.
doi: 10.2106/jbjs.18.00193

13. Ansari S, Khorshidi S, Karkhaneh A. Engineering of gradient osteochondral tissue: from nature to lab. *Acta Biomater*. 2019;87:41-54.
doi: 10.1016/j.actbio.2019.01.071

14. Bedell ML, Wang Z, Hogan KJ, et al. The effect of multi-material architecture on the ex vivo osteochondral integration of bioprinted constructs. *Acta Biomater*. 2023;155:99-112.
doi: 10.1016/j.actbio.2022.11.014

15. McKee TJ, Perlman G, Morris M, Komarova SV. Extracellular matrix composition of connective tissues: a systematic review and meta-analysis. *Sci Rep*. 2019;9(1):10542.
doi: 10.1038/s41598-019-46896-0

16. Di Luca A, Szlazak K, Lorenzo-Moldero I, et al. Influencing chondrogenic differentiation of human mesenchymal stromal cells in scaffolds displaying a structural gradient in pore size. *Acta Biomater*. 2016;36:210-219.
doi: 10.1016/j.actbio.2016.03.014

17. Shen G. The role of type X collagen in facilitating and regulating endochondral ossification of articular cartilage. *Orthod Craniofac Res*. 2005;8(1):11-17.
doi: 10.1111/j.1601-6343.2004.00308.x

18. Horkay F, Basser PJ, Geissler E. Cartilage extracellular matrix polymers: hierarchical structure, osmotic properties, and function. *Soft Matter*. 2024;20(30):6033-6043.
doi: 10.1039/d4sm00617h

19. Rose FR, Oreffo RO. Bone tissue engineering: hope vs hype. *Biochem Biophys Res Commun*. 2002;292(1):1-7.
doi: 10.1006/bbrc.2002.6519

20. Gonzalez-Fernandez T, Rathan S, Hobbs C, et al. Pore-forming bioinks to enable spatio-temporally defined gene delivery in bioprinted tissues. *J Control Release*. 2019;301:13-27.
doi: 10.1016/j.jconrel.2019.03.006

21. Rowland CR, Glass KA, Ettyreddy AR, et al. Regulation of decellularized tissue remodeling via scaffold-mediated lentiviral delivery in anatomically-shaped osteochondral constructs. *Biomaterials*. 2018;177:161-175.
doi: 10.1016/j.biomaterials.2018.04.049

22. Liu Y, Huang C, Bai M, Pi C, Zhang D, Xie J. The roles of Runx1 in skeletal development and osteoarthritis: a concise review. *Heliyon*. 2022;8(12):e12656.
doi: 10.1016/j.heliyon.2022.e12656

23. Li W, Zhang S, Liu J, Liu Y, Liang Q. Vitamin K2 stimulates MC3T3-E1 osteoblast differentiation and mineralization through autophagy induction. *Mol Med Rep*. 2019;19(5):3676-3684.
doi: 10.3892/mmr.2019.10040

24. Grogan SP, Duffy SF, Pauli C, et al. Zone-specific gene expression patterns in articular cartilage. *Arthritis Rheum*. 2013;65(2):418-428.
doi: 10.1002/art.37760

25. Zuscik MJ, Hilton MJ, Zhang X, Chen D, O'Keefe RJ. Regulation of chondrogenesis and chondrocyte differentiation by stress. *J Clin Invest*. 2008;118(2):429-438.
doi: 10.1172/jci34174

26. Ma J, Wang Z, Zhao J, Miao W, Ye T, Chen A. Resveratrol attenuates lipopolysaccharides (LPS)-induced inhibition of osteoblast differentiation in MC3T3-E1 cells. *Med Sci Monit*. 2018;24:2045-2052.
doi: 10.12659/msm.905703

27. Kitaura H, Marahleh A, Ohori F, et al. Osteocyte-related cytokines regulate osteoclast formation and bone resorption. *Int J Mol Sci*. 2020;21(14):5169.
doi: 10.3390/ijms21145169

28. Zhang D, Deng X, Liu Y, et al. MMP-10 deficiency effects differentiation and death of chondrocytes associated with endochondral osteogenesis in an endemic osteoarthritis. *Cartilage*. 2022;13(3):19476035221109226.
doi: 10.1177/19476035221109226

29. Boyce BF, Xing L. Functions of RANKL/RANK/OPG in bone modeling and remodeling. *Arch Biochem Biophys*. 2008;473(2):139-146.
doi: 10.1016/j.abb.2008.03.018

30. Quinn TM, Häuselmann HJ, Shintani N, Hunziker EB. Cell and matrix morphology in articular cartilage from adult human knee and ankle joints suggests depth-associated adaptations to biomechanical and anatomical roles. *Osteoarthritis Cartilage*. 2013;21(12):1904-1912.

31. Niu H, Liu C, Li A, et al. Relationship between triphasic mechanical properties of articular cartilage and osteoarthritic grade. *Sci China Life Sci*. 2012;55(5):444-451. doi: 10.1007/s11427-012-4326-7

32. Sun Y, Zhang K, Dong H, et al. Layered mechanical and electrical properties of porcine articular cartilage. *Med Biol Eng Comput*. 2022;60(10):3019-3028. doi: 10.1007/s11517-022-02653-6

33. Burr DB, Gallant MA. Bone remodelling in osteoarthritis. *Nat Rev Rheumatol*. 2012;8(11):665-673. doi: 10.1038/nrrheum.2012.130

34. Flachsmann ER, Broom ND, Oloyede A. A biomechanical investigation of unconstrained shear failure of the osteochondral region under impact loading. *Clin Biomech (Bristol)*. 1995;10(3):156-165. doi: 10.1016/0268-0033(95)93706-y

35. Madry H, van Dijk CN, Mueller-Gerbl M. The basic science of the subchondral bone. *Knee Surg Sports Traumatol Arthrosc*. 2010;18(4):419-433. doi: 10.1007/s00167-010-1054-z

36. Broom ND, Oloyede A, Flachsmann R, Hows M. Dynamic fracture characteristics of the osteochondral junction undergoing shear deformation. *Med Eng Phys*. 1996;18(5):396-404. doi: 10.1016/1350-4533(95)00067-4

37. Mieloch AA, Richter M, Trzeciak T, Giersig M, Rybka JD. Osteoarthritis severely decreases the elasticity and hardness of knee joint cartilage: a nanoindentation study. *J Clin Med*. 2019;8(11):1865. doi: 10.3390/jcm8111865

38. Davis S, Zekonyte J, Karali A, Roldo M, Blunn G. Early degenerative changes in a spontaneous osteoarthritis model assessed by nanoindentation. *Bioengineering (Basel)*. 2023;10(9):995. doi: 10.3390/bioengineering10090995

39. Peters AE, Akhtar R, Comerford EJ, Bates KT. The effect of ageing and osteoarthritis on the mechanical properties of cartilage and bone in the human knee joint. *Sci Rep*. 2018;8(1):5931. doi: 10.1038/s41598-018-24258-6

40. Hu YJ, Yu YE, Cooper HJ, et al. Mechanical and structural properties of articular cartilage and subchondral bone in human osteoarthritic knees. *J Bone Miner Res*. 2024;39(8):1120-1131. doi: 10.1093/jbmr/zjae094

41. Guo J, Li Q, Zhang R, et al. Loose pre-cross-linking mediating cellulose self-assembly for 3D printing strong and tough biomimetic scaffolds. *Biomacromolecules*. 2022;23(3):877-888. doi: 10.1021/acs.biomac.1c01330

42. Zhang X, Liu Y, Zuo Q, et al. 3D bioprinting of biomimetic bilayered scaffold consisting of decellularized extracellular matrix and silk fibroin for osteochondral repair. *Int J Bioprint*. 2021;7(4):401. doi: 10.18063/ijb.v7i4.401

43. Nedrelow DS, Rassi A, Ajeeb B, et al. Regenerative engineering of a biphasic patient-fitted temporomandibular joint condylar prosthesis. *Tissue Eng Part C Methods*. 2023;29(7):307-320. doi: 10.1089/ten.TEC.2023.0093

44. Wu Z, Yao H, Sun H, et al. Enhanced hyaline cartilage formation and continuous osteochondral regeneration via 3D-Printed heterogeneous hydrogel with multi-crosslinking inks. *Mater Today Bio*. 2024;26:101080. doi: 10.1016/j.mtbio.2024.101080

45. Diloksumpan P, de Ruijter M, Castilho M, et al. Combining multi-scale 3D printing technologies to engineer reinforced hydrogel-ceramic interfaces. *Biofabrication*. 2020;12(2):025014. doi: 10.1088/1758-5090/ab69d9

46. Liu Y, Peng L, Li L, et al. 3D-bioprinted BMSC-laden biomimetic multiphasic scaffolds for efficient repair of osteochondral defects in an osteoarthritic rat model. *Biomaterials*. 2021;279:121216. doi: 10.1016/j.biomaterials.2021.121216

47. Gao J, Ding X, Yu X, et al. Cell-free bilayered porous scaffolds for osteochondral regeneration fabricated by continuous 3d-printing using nascent physical hydrogel as ink. *Adv Healthc Mater*. 2021;10(3):e2001404. doi: 10.1002/adhm.202001404

48. Wang Z, Cao W, Wu F, et al. A triphasic biomimetic BMSC-loaded scaffold for osteochondral integrated regeneration in rabbits and pigs. *Biomater Sci*. 2023;11(8):2924-2934. doi: 10.1039/d2bm02148j

49. Braxton T, Lim K, Alcala-Orozco C, et al. Mechanical and physical characterization of a biphasic 3D printed silk-infilled scaffold for osteochondral tissue engineering. *ACS Biomater Sci Eng*. 2024;10(12):7606-7618. doi: 10.1021/acsbiomaterials.4c01865

50. Wang S, Luo B, Bai B, et al. 3D printed chondrogenic functionalized PGS bioactive scaffold for cartilage regeneration. *Adv Healthc Mater*. 2023;12(27): e2301006. doi: 10.1002/adhm.202301006

51. Wang H, Zhang J, Bai H, et al. 3D printed cell-free bilayer porous scaffold based on alginate with biomimetic microenvironment for osteochondral defect repair. *Biomater Adv*. 2025;167:214092. doi: 10.1016/j.bioadv.2024.214092

52. Ding X, Gao J, Yu X, et al. 3D-printed porous scaffolds of hydrogels modified with TGF-β1 binding peptides to promote in vivo cartilage regeneration and animal gait restoration. *ACS Appl Mater Interfaces*. 2022;14(14):15982-15995. doi: 10.1021/acsami.2c00761

53. Li Q, Yu H, Zhao F, et al. 3D printing of microenvironment-specific bioinspired and exosome-reinforced hydrogel scaffolds for efficient cartilage and subchondral bone regeneration. *Adv Sci (Weinh)*. 2023;10(26):e2303650. doi: 10.1002/advs.202303650

54. Cui X, Alcala-Orozco CR, Baer K, et al. 3D bioassembly of cell-instructive chondrogenic and osteogenic hydrogel microspheres containing allogeneic stem cells for hybrid biofabrication of osteochondral constructs. *Biofabrication*. 2022;14(3):034101. doi: 10.1088/1758-5090/ac61a3

55. Wei W, Liu W, Kang H, et al. A one-stone-two-birds strategy for osteochondral regeneration based on a 3D printable biomimetic scaffold with kartogenin biochemical stimuli gradient. *Adv Healthc Mater*. 2023;12(15):e2300108. doi: 10.1002/adhm.202300108

56. Coyle A, Chakraborty A, Huang J, Shamiya Y, Luo W, Paul A. In vitro engineered ECM-incorporated hydrogels for osteochondral tissue repair: a cell-free approach. *Adv Healthc Mater*. 2025;14(4):e2402701. doi: 10.1002/adhm.202402701

57. Sun T, Feng Z, He W, et al. Novel 3D-printing bilayer GelMA-based hydrogel containing BP,β-TCP and exosomes for cartilage-bone integrated repair. *Biofabrication*. 2023;16(1):015008. doi: 10.1088/1758-5090/ad04fe

58. Eckstein KN, Hergert JE, Uzcategui AC, et al. Controlled mechanical property gradients within a digital light processing printed hydrogel-composite osteochondral scaffold. *Ann Biomed Eng*. 2024;52(8):2162-2177. doi: 10.1007/s10439-024-03516-x

59. Golebiowska A, Nukavarapu SP. Bio-inspired zonal-structured matrices for bone-cartilage interface engineering. *Biofabrication*. 2022;14(2):025016. doi: 10.1088/1758-5090/ac52e1

60. Sun Y, Wu Q, Zhang Y, Dai K, Wei Y. 3D-bioprinted gradient-structured scaffold generates anisotropic cartilage with vascularization by pore-size-dependent activation of HIF1α/FAK signaling axis. *Nanomedicine*. 2021; 37:102426. doi: 10.1016/j.nano.2021.102426

61. Gu Y, Zou Y, Huang Y, et al. 3D-printed biomimetic scaffolds with precisely controlled and tunable structures guide cell migration and promote regeneration of osteochondral defect. *Biofabrication*. 2023;16(1):015003. doi: 10.1088/1758-5090/ad0071

62. Kilian D, Cometta S, Bernhardt A, et al. Core-shell bioprinting as a strategy to apply differentiation factors in a spatially defined manner inside osteochondral tissue substitutes. *Biofabrication*. 2022;14(1):014108. doi: 10.1088/1758-5090/ac457b

63. Zhang Y, Li D, Liu Y, et al. 3D-bioprinted anisotropic bicellular living hydrogels boost osteochondral regeneration via reconstruction of cartilage-bone interface. *Innovation (Camb)*. 2024;5(1):100542. doi: 10.1016/j.xinn.2023.100542

64. Maherani M, Eslami H, Poursamar SA, Ansari M. A modular approach to 3D-printed bilayer composite scaffolds for osteochondral tissue engineering. *J Mater Sci Mater Med*. 2024;35(1):62. doi: 10.1007/s10856-024-06824-9

65. O'Shea DG, Hodgkinson T, Curtin CM, O'Brien FJ. An injectable and 3D printable pro-chondrogenic hyaluronic acid and collagen type II composite hydrogel for the repair of articular cartilage defects. *Biofabrication*. 2023;16(1):015007. doi: 10.1088/1758-5090/ad047a

66. Zineh BR, Roshangar L, Meshgi S, Shabgard M. 3D printing of alginate/thymoquinone/halloysite nanotube bio-scaffolds for cartilage repairs: experimental and numerical study. *Med Biol Eng Comput*. 2022;60(11):3069-3080. doi: 10.1007/s11517-022-02654-5

67. Naranda J, Bračič M, Vogrin M, Maver U. Recent advancements in 3d printing of polysaccharide hydrogels in cartilage tissue engineering. *Materials (Basel)*. 2021;14(14):3977. doi: 10.3390/ma14143977

68. Majumder N, Roy C, Doenges L, Martin I, Barbero A, Ghosh S. Covalent conjugation of small molecule inhibitors and growth factors to a silk fibroin-derived bioink to develop phenotypically stable 3D bioprinted cartilage. *ACS Appl Mater Interfaces*. 2024;16(8):9925-9943. doi: 10.1021/acsami.3c18903

69. Zhang W, Lian Q, Li D, et al. Cartilage repair and subchondral bone migration using 3D printing osteochondral composites: a one-year-period study in rabbit trochlea. *Biomed Res Int*. 2014;2014:746138. doi: 10.1155/2014/746138

70. Golebiowska AA, Nukavarapu SP. Bio-inspired zonal-structured matrices for bone-cartilage interface engineering. *Biofabrication*. 2022;14(2):025016. doi: 10.1088/1758-5090/ac5413

71. Jiang G, Li S, Yu K, et al. A 3D-printed PRP-GelMA hydrogel promotes osteochondral regeneration through M2 macrophage polarization in a rabbit model. *Acta Biomater*. 2021;128:150-162. doi: 10.1016/j.actbio.2021.04.010

72. Parisi C, Salvatore L, Veschini L, et al. Biomimetic gradient scaffold of collagen-hydroxyapatite for osteochondral regeneration. *J Tissue Eng*. 2020;11:2041731419896068. doi: 10.1177/2041731419896068

73. Sa MW, Nguyen BB, Moriarty RA, Kamalitdinov T, Fisher JP, Kim JY. Fabrication and evaluation of 3D printed BCP scaffolds reinforced with ZrO(2) for bone tissue applications. *Biotechnol Bioeng*. 2018;115(4):989-999. doi: 10.1002/bit.26514

74. Liu L, Yu F, Chen L, Xia L, Wu C, Fang B. Lithium-containing biomaterials stimulate cartilage repair through bone marrow stromal cells-derived exosomal miR-455-3p and Histone H3 acetylation. *Adv Healthc Mater*. 2023;12(11):e2202390. doi: 10.1002/adhm.202202390

75. Zheng J, Mao X, Ling J, Chen C, Zhang W. Role of magnesium transporter subtype 1 (MagT1) in the osteogenic differentiation of rat bone marrow stem cells. *Biol Trace Elem Res*. 2016;171(1):131-137. doi: 10.1007/s12011-015-0459-4

76. Wang X, Gao L, Han Y, et al. Silicon-enhanced adipogenesis and angiogenesis for vascularized adipose tissue engineering. *Adv Sci (Weinh)*. 2018;5(11):1800776. doi: 10.1002/advs.201800776

77. Rahaman MN, Day DE, Bal BS, et al. Bioactive glass in tissue engineering. *Acta Biomater*. 2011;7(6):2355-2373. doi: 10.1016/j.actbio.2011.03.016

78. Morgan EF, Salisbury Palomares KT, Gleason RE, et al. Correlations between local strains and tissue phenotypes in an experimental model of skeletal healing. *J Biomech*. 2010;43(12):2418-2424. doi: 10.1016/j.jbiomech.2010.04.019

79. Claes L, Eckert-Hübner K, Augat P. The effect of mechanical stability on local vascularization and tissue differentiation in callus healing. *J Orthop Res*. 2002;20(5):1099-1105. doi: 10.1016/s0736-0266(02)00044-x

80. Chen C, Xie J, Deng L, Yang L. Substrate stiffness together with soluble factors affects chondrocyte mechanoresponses. *ACS Appl Mater Interfaces*. 2014;6(18):16106-16116. doi: 10.1021/am504135b

81. Yang Y, Feng Y, Qu R, et al. Synthesis of aligned porous polyethylene glycol/silk fibroin/hydroxyapatite scaffolds for osteoinduction in bone tissue engineering. *Stem Cell Res Ther*. 2020;11(1):522. doi: 10.1186/s13287-020-02024-8

82. Cao B, Li J, Wang X, et al. Mechanosensitive miR-99b mediates the regulatory effect of matrix stiffness on bone marrow mesenchymal stem cell fate both in vitro and in vivo. *APL Bioeng*. 2023;7(1):016106. doi: 10.1063/5.0131125

83. Lai Q, Li B, Chen L, Zhou Y, Bao H, Li H. Substrate stiffness regulates the proliferation and inflammation of chondrocytes and macrophages through exosomes. *Acta Biomater*. 2025;192:77-89. doi: 10.1016/j.actbio.2024.12.021

84. Tortorici M, Petersen A, Ehrhart K, Duda GN, Checa S. Scaffold-dependent mechanical and architectural cues guide osteochondral defect healing in silico. *Front Bioeng Biotechnol*. 2021;9:642217. doi: 10.3389/fbioe.2021.642217

85. Radhakrishnan J, Manigandan A, Chinnaswamy P, Subramanian A, Sethuraman S. Gradient nano-engineered in situ forming composite hydrogel for osteochondral regeneration. *Biomaterials*. 2018;162:82-98. doi: 10.1016/j.biomaterials.2018.01.056

86. Pattnaik A, Sanket AS, Pradhan S, et al. Designing of gradient scaffolds and their applications in tissue regeneration. *Biomaterials*. 2023;296:122078. doi: doi: 10.1016/j.biomaterials.2023.122078

87. Zhang W, Chen J, Tao J, et al. The use of type 1 collagen scaffold containing stromal cell-derived factor-1 to create a matrix environment conducive to partial-thickness cartilage defects repair. *Biomaterials*. 2013;34(3):713-723. doi: 10.1016/j.biomaterials.2012.10.027

88. Hayashi K, Shimabukuro M, Kishida R, Tsuchiya A, Ishikawa K. Honeycomb scaffolds capable of achieving barrier membrane-free guided bone regeneration. *Mater Adv*. 2021;2(23):7638-7649. doi: 10.1039/D1MA00698C

89. Zhao Y, Liang Y, Ding S, Zhang K, Mao HQ, Yang Y. Application of conductive PPy/SF composite scaffold and electrical stimulation for neural tissue engineering. *Biomaterials*. 2020;255:120164. doi: 10.1016/j.biomaterials.2020.120164

90. He J, Sun C, Gu Z, et al. Morphology, migration, and transcriptome analysis of schwann cell culture on butterfly wings with different surface architectures. *ACS Nano*. 2018;12(10):9660-9668. doi: 10.1021/acsnano.8b00552

91. Zhang J, Wu Y, Thote T, Lee EH, Ge Z, Yang Z. The influence of scaffold microstructure on chondrogenic differentiation of mesenchymal stem cells. *Biomed Mater*. 2014;9(3):035011. doi: 10.1088/1748-6041/9/3/035011

92. DeLise AM, Fischer L, Tuan RS. Cellular interactions and signaling in cartilage development. *Osteoarthritis Cartilage*. 2000;8(5):309-334. doi: 10.1053/joca.1999.0306

93. Li S, Tallia F, Mohammed AA, Stevens MM, Jones JR. Scaffold channel size influences stem cell differentiation pathway in 3-D printed silica hybrid scaffolds for cartilage regeneration. *Biomater Sci*. 2020;8(16):4458-4466. doi: 10.1039/c9bm01829h

94. Zanetti NC, Solursh M. Induction of chondrogenesis in limb mesenchymal cultures by disruption of the actin cytoskeleton. *J Cell Biol*. 1984;99(1 Pt 1):115-123. doi: 10.1083/jcb.99.1.115

95. Vanden Berg-Foels WS. In situ tissue regeneration: chemoattractants for endogenous stem cell recruitment. *Tissue Eng Part B Rev*. 2014;20(1):28-39.

doi: 10.1089/ten.TEB.2013.0100

96. Salgado AJ, Coutinho OP, Reis RL. Bone tissue engineering: state of the art and future trends. *Macromol Biosci*. 2004;4(8):743-765. doi: 10.1002/mabi.200400026

97. Zhang X, Chen X, Hong H, Hu R, Liu J, Liu C. Decellularized extracellular matrix scaffolds: recent trends and emerging strategies in tissue engineering. *Bioact Mater*. 2022;10:15-31. doi: 10.1016/j.bioactmat.2021.09.014

98. Jang J, Kim TG, Kim BS, Kim SW, Kwon SM, Cho DW. Tailoring mechanical properties of decellularized extracellular matrix bioink by vitamin B2-induced photo-crosslinking. *Acta Biomater*. 2016;33:88-95. doi: 10.1016/j.actbio.2016.01.013

99. Zhang X, Liu Y, Luo C, et al. Crosslinker-free silk/decellularized extracellular matrix porous bioink for 3D bioprinting-based cartilage tissue engineering. *Mater Sci Eng C Mater Biol Appl*. 2021;118:111388. doi: 10.1016/j.msec.2020.111388

100. Joyce M, Hodgkinson T, Lemoine M, González-Vázquez A, Kelly DJ, O'Brien FJ. Development of a 3D-printed bioabsorbable composite scaffold with mechanical properties suitable for treating large, load-bearingarticular cartilage defects. *Eur Cell Mater*. 2023;45:158-172. doi: 10.22203/eCM.v045a11

101. Johnson K, Zhu S, Tremblay MS, et al. A stem cell-based approach to cartilage repair. *Science*. 2012;336(6082):717-721. doi: 10.1126/science.1215157

102. Stefani RM, Lee AJ, Tan AR, et al. Sustained low-dose dexamethasone delivery via a PLGA microsphere-embedded agarose implant for enhanced osteochondral repair. *Acta Biomaterialia*. 2020;102:326-340. doi: doi: 10.1016/j.actbio.2019.11.052

103. Brito Barrera YA, Husteden C, Alherz J, Fuhrmann B, Wölk C, Groth T. Extracellular matrix-inspired surface coatings functionalized with dexamethasone-loaded liposomes to induce osteo- and chondrogenic differentiation of multipotent stem cells. *Mater Sci Eng C Mater Biol Appl*. 2021;131:112516. doi: 10.1016/j.msec.2021.112516

104. Yan X, Chen YR, Song YF, et al. Scaffold-based gene therapeutics for osteochondral tissue engineering. *Front Pharmacol*. 2019;10:1534. doi: 10.3389/fphar.2019.01534

105. An C, Cheng Y, Yuan Q, Li J. IGF-1 and BMP-2 induces differentiation of adipose-derived mesenchymal stem cells into chondrocytes-like cells. *Ann Biomed Eng*. 2010;38(4):1647-1654. doi: 10.1007/s10439-009-9892-x

106. Tao K, Frisch J, Rey-Rico A, et al. Co-overexpression of TGF-β and SOX9 via rAAV gene transfer modulates the metabolic and chondrogenic activities of human bone marrow-derived mesenchymal stem cells. *Stem Cell Res Ther*. 2016;7:20. doi: 10.1186/s13287-016-0280-9

107. Lee JM, Im GI. SOX trio-co-transduced adipose stem cells in fibrin gel to enhance cartilage repair and delay the progression of osteoarthritis in the rat. *Biomaterials*. 2012;33(7):2016-2024. doi: 10.1016/j.biomaterials.2011.11.050

108. Vermeij EA, Broeren MG, Bennink MB, et al. Disease-regulated local IL-10 gene therapy diminishes synovitis and cartilage proteoglycan depletion in experimental arthritis. *Ann Rheum Dis*. 2015;74(11):2084-2091. doi: 10.1136/annrheumdis-2014-205223

109. Kay JD, Gouze E, Oligino TJ, et al. Intra-articular gene delivery and expression of interleukin-1Ra mediated by self-complementary adeno-associated virus. *J Gene Med*. 2009;11(7):605-614. doi: 10.1002/jgm.1334

110. Bellavia D, Veronesi F, Carina V, et al. Gene therapy for chondral and osteochondral regeneration: is the future now? *Cell Mol Life Sci*. 2018;75(4):649-667. doi: 10.1007/s00018-017-2637-3

111. Lu H, Wei J, Liu K, et al. Radical-scavenging and subchondral bone-regenerating nanomedicine for osteoarthritis treatment. *ACS Nano*. 2023;17(6):6131-6146. doi: 10.1021/acsnano.3c01789

112. Chen Y, Huang H, Zhong W, Li L, Lu Y, Si HB. miR-140-5p protects cartilage progenitor/stem cells from fate changes in knee osteoarthritis. *Int Immunopharmacol*. 2023;114:109576. doi: 10.1016/j.intimp.2022.109576

113. Xing H, Zhang Z, Mao Q, et al. Injectable exosome-functionalized extracellular matrix hydrogel for metabolism balance and pyroptosis regulation in intervertebral disc degeneration. *J Nanobiotechnol*. 2021;19(1):264. doi: 10.1186/s12951-021-00991-5

114. Zhu W, Wang H, Feng B, et al. Self-healing hyaluronic acid-based hydrogel with miRNA140-5p loaded MON-PEI nanoparticles for chondrocyte regeneration: Schiff base self-assembly approach. *Adv Sci (Weinh)*. 2025;12(1):e2406479. doi: 10.1002/advs.202406479

115. Tuan RS, Chen AF, Klatt BA. Cartilage regeneration. *J Am Acad Orthop Surg*. 2013;21(5):303-311. doi: 10.5435/jaaos-21-05-303

116. Wang LT, Ting CH, Yen ML, et al. Human mesenchymal stem cells (MSCs) for treatment towards immune- and inflammation-mediated diseases: review of current clinical trials. *J Biomed Sci*. 2016;23(1):76. doi: 10.1186/s12929-016-0289-5

117. Bush CJ, Grant JA, Krych AJ, Bedi A. The role of mesenchymal stromal cells in the management of knee chondral defects. *J Bone Joint Surg Am*. 2022;104(3):284-292.

doi: 10.2106/jbjs.20.01800

118. Armiento AR, Alini M, Stoddart MJ. Articular fibrocartilage - why does hyaline cartilage fail to repair? *Adv Drug Deliv Rev*. 2019;146:289-305.
doi: 10.1016/j.addr.2018.12.015

119. Knutsen G, Engebretsen L, Ludvigsen TC, et al. Autologous chondrocyte implantation compared with microfracture in the knee. A randomized trial. *J Bone Joint Surg Am*. 2004;86(3):455-464.
doi: 10.2106/00004623-200403000-00001

120. Zhen G, Wen C, Jia X, et al. Inhibition of TGF-β signaling in mesenchymal stem cells of subchondral bone attenuates osteoarthritis. *Nat Med*. 2013;19(6):704-712.
doi: 10.1038/nm.3143

121. Lam J, Lu S, Kasper FK, Mikos AG. Strategies for controlled delivery of biologics for cartilage repair. *Adv Drug Deliv Rev*. 2015;84:123-134.
doi: doi: 10.1016/j.addr.2014.06.006

122. Möller T, Amoroso M, Hägg D, et al. In vivo chondrogenesis in 3d bioprinted human cell-laden hydrogel constructs. *Plast Reconstr Surg Glob Open*. 2017;5(2):e1227.
doi: 10.1097/gox.0000000000001227

123. Wu H, Wang X, Wang G, et al. Advancing scaffold-assisted modality for in situ osteochondral regeneration: a shift from biodegradable to bioadaptable. *Adv Mater*. 2024;36(47):e2407040.
doi: 10.1002/adma.202407040

124. Karageorgiou V, Kaplan D. Porosity of 3D biomaterial scaffolds and osteogenesis. *Biomaterials*. 2005;26(27): 5474-5491.
doi: 10.1016/j.biomaterials.2005.02.002

125. Brauer DS. Bioactive glasses—structure and properties. *Angew Chem Int Ed Engl*. 2015;54(14):4160-4181.
doi: 10.1002/anie.201405310

126. Bejarano J, Boccaccini AR, Covarrubias C, Palza H. Effect of Cu- and Zn-doped bioactive glasses on the in vitro bioactivity, mechanical and degradation behavior of biodegradable PDLLA scaffolds. *Materials (Basel)*. 2020;13(13):2908.
doi: 10.3390/ma13132908

127. Heiden M, Nauman E, Stanciu L. Bioresorbable Fe–Mn and Fe–Mn–HA materials for orthopedic implantation: enhancing degradation through porosity control. *Adv Healthc Mater*. 2017;6(13):1700120.
doi: doi: 10.1002/adhm.201700120

128. Kim JA, Lim J, Naren R, Yun HS, Park EK. Effect of the biodegradation rate controlled by pore structures in magnesium phosphate ceramic scaffolds on bone tissue regeneration in vivo. *Acta Biomater*. 2016;44:155-167.
doi: 10.1016/j.actbio.2016.08.039

129. Qu Z, Liu L, Deng Y, et al. Relationship between biodegradation rate and grain size itself excluding other structural factors caused by alloying additions and deformation processing for pure Mg. *Materials (Basel)*. 2022;15(15):5295.
doi: 10.3390/ma15155295

130. Hu Q, Ecker M. Overview of MMP-13 as a promising target for the treatment of osteoarthritis. *Int J Mol Sci*. 2021;22(4):1742.
doi: 10.3390/ijms22041742

131. Choe R, Devoy E, Jabari E, Packer JD, Fisher JP. Biomechanical aspects of osteochondral regeneration: implications and strategies for three-dimensional bioprinting. *Tissue Eng Part B Rev*. 2022;28(4):766-788.
doi: 10.1089/ten.TEB.2021.0101

132. Knudson W, Casey B, Nishida Y, Eger W, Kuettner KE, Knudson CB. Hyaluronan oligosaccharides perturb cartilage matrix homeostasis and induce chondrocytic chondrolysis. *Arthritis Rheum*. 2000;43(5):1165-1174.
doi: 10.1002/1529-0131(200005)43:5<1165::Aid-anr27>3.0.Co;2-h

133. Yildirim N, Amanzhanova A, Kulzhanova G, Mukasheva F, Erisken C. Osteochondral interface: regenerative engineering and challenges. *ACS Biomater Sci Eng*. 2023;9(3):1205-1223.
doi: 10.1021/acsbiomaterials.2c01321

134. Kamaraj M, Roopavath UK, Giri PS, Ponnusamy NK, Rath SN. Modulation of 3D printed calcium-deficient apatite constructs with varying mn concentrations for osteochondral regeneration via endochondral differentiation. *ACS Appl Mater Interfaces*. 2022;14(20):23245-23259.
doi: 10.1021/acsami.2c05110

135. Liuyun J, Lixin J, Chengdong X, Lijuan X, Ye L. Effect of l-lysine-assisted surface grafting for nano-hydroxyapatite on mechanical properties and in vitro bioactivity of poly(lactic acid-co-glycolic acid). *J Biomater Appl*. 2016;30(6):750-758.
doi: 10.1177/0885328215584491

136. Nedrelow DS, Townsend JM, Detamore MS. Osteochondral regeneration with anatomical scaffold 3D-printing-design considerations for interface integration. *J Biomed Mater Res A*. 2025;113(1):e37804.
doi: 10.1002/jbm.a.37804

137. Brown WE, Huang BJ, Hu JC, Athanasiou KA. Engineering large, anatomically shaped osteochondral constructs with robust interfacial shear properties. *NPJ Regen Med*. 2021;6(1):42.
doi: 10.1038/s41536-021-00152-0

138. Feng P, He J, Peng S, et al. Characterizations and interfacial reinforcement mechanisms of multicomponent biopolymer based scaffold. *Mater Sci Eng C Mater Biol Appl*. 2019;100:809-825.
doi: 10.1016/j.msec.2019.03.030

139. Wang L, Zhao L, Detamore MS. Human umbilical cord mesenchymal stromal cells in a sandwich approach for osteochondral tissue engineering. *J Tissue Eng Regen Med*. 2011;5(9):712-721.
doi: 10.1002/term.370

140. Li S, Liu C, Zhang Y, et al. Continuous 3D printing of biomimetic beetle mandible structure with long bundles of aramid fiber composites. *Biomimetics (Basel)*. 2023;8(3):283. doi: 10.3390/biomimetics8030283

141. Yodmuang S, Guo H, Brial C, et al. Effect of interface mechanical discontinuities on scaffold-cartilage integration. *J Orthop Res*. 2019;37(4):845-854. doi: 10.1002/jor.24238

142. Zhao R, Han F, Yu Q, et al. A multifunctional scaffold that promotes the scaffold-tissue interface integration and rescues the ROS microenvironment for repair of annulus fibrosus defects. *Bioact Mater*. 2024;41:257-270. doi: 10.1016/j.bioactmat.2024.03.007

143. Torres-Claramunt R, Martínez-Díaz S, Sánchez-Soler JF, et al. Fibronectin-coated polyurethane meniscal scaffolding supplemented with MSCs improves scaffold integration and proteoglycan production in a rabbit model. *Knee Surg Sports Traumatol Arthrosc*. 2023;31(11):5104-5110. doi: 10.1007/s00167-023-07562-1

144. Chung JY, Song M, Ha CW, Kim JA, Lee CH, Park YB. Comparison of articular cartilage repair with different hydrogel-human umbilical cord blood-derived mesenchymal stem cell composites in a rat model. *Stem Cell Res Ther*. 2014;5(2):39. doi: 10.1186/scrt427

145. Romito L, Ameer GA. Mechanical interlocking of engineered cartilage to an underlying polymeric substrate: towards a biohybrid tissue equivalent. *Ann Biomed Eng*. 2006;34(5):737-747. doi: 10.1007/s10439-006-9089-5

146. Scotti C, Wirz D, Wolf F, et al. Engineering human cell-based, functionally integrated osteochondral grafts by biological bonding of engineered cartilage tissues to bony scaffolds. *Biomaterials*. 2010;31(8):2252-2259. doi: 10.1016/j.biomaterials.2009.11.110

147. Ege D, Hasirci V. Is 3D printing promising for osteochondral tissue regeneration? *ACS Appl Bio Mater*. 2023;6(4):1431-1444. doi: 10.1021/acsabm.3c00093

148. Jammalamadaka U, Tappa K. Recent advances in biomaterials for 3d printing and tissue engineering. *J Funct Biomater*. 2018;9(1):22. doi: 10.3390/jfb9010022

149. Steinmetz NJ, Aisenbrey EA, Westbrook KK, Qi HJ, Bryant SJ. Mechanical loading regulates human MSC differentiation in a multi-layer hydrogel for osteochondral tissue engineering. *Acta Biomater*. 2015;21:142-153. doi: 10.1016/j.actbio.2015.04.015

150. Kilian D, Ahlfeld T, Akkineni AR, Bernhardt A, Gelinsky M, Lode A. 3D Bioprinting of osteochondral tissue substitutes - in vitro-chondrogenesis in multi-layered mineralized constructs. *Sci Rep*. 2020;10(1):8277. doi: 10.1038/s41598-020-65050-9

151. Gong L, Li J, Zhang J, et al. An interleukin-4-loaded bi-layer 3D printed scaffold promotes osteochondral regeneration. *Acta Biomater*. 2020;117:246-260. doi: 10.1016/j.actbio.2020.09.039

152. Senior JJ, Cooke ME, Grover LM, Smith AM. Fabrication of complex hydrogel structures using suspended layer additive manufacturing (SLAM). *Adv Funct Mater*. 2019;29(49):1904845. doi: doi: 10.1002/adfm.201904845

153. Uzcategui AC, Muralidharan A, Ferguson VL, Bryant SJ, McLeod RR. Understanding and improving mechanical properties in 3D printed parts using a dual-cure acrylate-based resin for stereolithography. *Adv Eng Mater*. 2018;20(12);1800876. doi: 10.1002/adem.201800876

154. Li X, Liu B, Pei B, et al. Inkjet bioprinting of biomaterials. *Chem Rev*. 2020;120(19):10793-10833. doi: 10.1021/acs.chemrev.0c00008

155. Dufour A, Gallostra XB, O'Keeffe C, et al. Integrating melt electrowriting and inkjet bioprinting for engineering structurally organized articular cartilage. *Biomaterials*. 2022;283:121405. doi: 10.1016/j.biomaterials.2022.121405

156. Li Q, Xu S, Feng Q, et al. 3D printed silk-gelatin hydrogel scaffold with different porous structure and cell seeding strategy for cartilage regeneration. *Bioact Mater*. 2021;6(10):3396-3410. doi: 10.1016/j.bioactmat.2021.03.013

157. Ahn SH, Lee J, Park SA, Kim WD. Three-dimensional bio-printing equipment technologies for tissue engineering and regenerative medicine. *Tissue Eng Regen Med*. 2016;13(6):663-676. doi: 10.1007/s13770-016-0148-1

158. Della Bona A, Cantelli V, Britto VT, Collares KF, Stansbury JW. 3D printing restorative materials using a stereolithographic technique: a systematic review. *Dent Mater*. 2021;37(2):336-350. doi: 10.1016/j.dental.2020.11.030

159. Jeong M, Radomski K, Lopez D, Liu JT, Lee JD, Lee SJ. Materials and applications of 3D printing technology in dentistry: an overview. *Dent J (Basel)*. 2023;12(1):1. doi: 10.3390/dj12010001

160. Wang Y, Ling C, Chen J, et al. 3D-printed composite scaffold with gradient structure and programmed biomolecule delivery to guide stem cell behavior for osteochondral regeneration. *Biomater Adv*. 2022;140:213067. doi: 10.1016/j.bioadv.2022.213067

161. Cailleaux S, Sanchez-Ballester NM, Gueche YA, Bataille B, Soulairol I. Fused Deposition Modeling (FDM), the new asset for the production of tailored medicines. *J Control Release*. 2021;330:821-841. doi: 10.1016/j.jconrel.2020.10.056

162. Jia W, Liu Z, Sun L, et al. A multicrosslinked network composite hydrogel scaffold based on DLP photocuring printing for nasal cartilage repair. *Biotechnol Bioeng*. 2024;121(9):2752-2766. doi: 10.1002/bit.28769

163. Choe R, Devoy E, Kuzemchak B, et al. Computational investigation of interface printing patterns within 3D printed multilayered scaffolds for osteochondral tissue engineering. *Biofabrication*. 2022;14(2):025015. doi: 10.1088/1758-5090/ac5220

164. Tamaddon M, Liu C. Enhancing biological and biomechanical fixation of osteochondral scaffold: a grand challenge. *Adv Exp Med Biol*. 2018;1059:255-298. doi: 10.1007/978-3-319-76735-2_12

165. Tamaddon M, Czernuszka J. The need for hierarchical scaffolds in bone tissue engineering. *Hard Tissue*. 2013;2:37. doi: 10.13172/2050-2303-2-4-773

166. Colosi C, Shin SR, Manoharan V, et al. Microfluidic bioprinting of heterogeneous 3D tissue constructs using low-viscosity bioink. *Adv Mater*. 2016;28(4):677-684. doi: 10.1002/adma.201503310

167. García-Fernández L. Osteochondral angiogenesis and promoted vascularization: new therapeutic target. *Adv Exp Med Biol*. 2018;1059:315-330. doi: 10.1007/978-3-319-76735-2_14

168. Sachlos E, Czernuszka JT. Making tissue engineering scaffolds work. Review: the application of solid freeform fabrication technology to the production of tissue engineering scaffolds. *Eur Cell Mater*. 2003;5:29-39; discussion 39-40. doi: 10.22203/ecm.v005a03

169. Perets A, Baruch Y, Weisbuch F, Shoshany G, Neufeld G, Cohen S. Enhancing the vascularization of three-dimensional porous alginate scaffolds by incorporating controlled release basic fibroblast growth factor microspheres. *J Biomed Mater Res A*. 2003;65(4):489-497. doi: 10.1002/jbm.a.10542

170. Li B, Wang H, Qiu G, Su X, Wu Z. Synergistic effects of vascular endothelial growth factor on bone morphogenetic proteins induced bone formation in vivo: influencing factors and future research directions. *Biomed Res Int*. 2016;2016:2869572. doi: 10.1155/2016/2869572

171. Centola M, Abbruzzese F, Scotti C, et al. Scaffold-based delivery of a clinically relevant anti-angiogenic drug promotes the formation of in vivo stable cartilage. *Tissue Eng Part A*. 2013;19(17-18):1960-1971. doi: 10.1089/ten.TEA.2012.0455

172. Firsching-Hauck A, Nickel P, Yahya C, et al. Angiostatic effects of suramin analogs in vitro. *Anticancer Drugs*. 2000;11(2):69-77. doi: 10.1097/00001813-200002000-00002

173. Qin C, Zhang H, Chen L, et al. Cell-laden scaffolds for vascular-innervated bone regeneration. *Adv Healthc Mater*. 2023;12(13):e2201923. doi: 10.1002/adhm.202201923

174. Liang X, Xie L, Zhang Q, et al. Gelatin methacryloyl-alginate core-shell microcapsules as efficient delivery platforms for prevascularized microtissues in endodontic regeneration. *Acta Biomater*. 2022;144:242-257. doi: 10.1016/j.actbio.2022.03.045

175. Lu X, Dai S, Huang B, et al. Exosomes loaded a smart bilayer-hydrogel scaffold with ROS-scavenging and macrophage-reprogramming properties for repairing cartilage defect. *Bioact Mater*. 2024;38:137-153. doi: 10.1016/j.bioactmat.2024.04.017

176. Xu M, Su T, Jin X, et al. Inflammation-mediated matrix remodeling of extracellular matrix-mimicking biomaterials in tissue engineering and regenerative medicine. *Acta Biomater*. 2022;151:106-117. doi: doi: 10.1016/j.actbio.2022.08.015

177. Shu C, Qin C, Chen L, et al. Metal-organic framework functionalized bioceramic scaffolds with antioxidative activity for enhanced osteochondral regeneration. *Adv Sci (Weinh)*. 2023;10(13):e2206875. doi: 10.1002/advs.202206875

178. Del Rio D, Stewart AJ, Pellegrini N. A review of recent studies on malondialdehyde as toxic molecule and biological marker of oxidative stress. *Nutr Metab Cardiovasc Dis*. 2005;15(4):316-328. doi: 10.1016/j.numecd.2005.05.003

179. Gu T, Zhang Z, Liu J, et al. Chlorogenic acid alleviates LPS-induced inflammation and oxidative stress by modulating CD36/AMPK/PGC-1α in RAW264.7 macrophages. *Int J Mol Sci*. 2023;24(17):13516. doi: 10.3390/ijms241713516

180. Vapniarsky N, Simpson DL, Arzi B, et al. Histological, immunological, and genetic analysis of feline chronic gingivostomatitis. *Front Vet Sci*. 2020;7:310. doi: 10.3389/fvets.2020.00310

181. Mata R, Yao Y, Cao W, et al. The dynamic inflammatory tissue microenvironment: signality and disease therapy by biomaterials. *Research (Wash D C)*. 2021; 2021:4189516. doi: 10.34133/2021/4189516

182. Li S, Niu D, Fang H, et al. Tissue adhesive, ROS scavenging and injectable PRP-based 'plasticine' for promoting cartilage repair. *Regen Biomater*. 2024;11:rbad104. doi: 10.1093/rb/rbad104

183. Liu D, Lu G, Shi B, et al. ROS-scavenging hydrogels synergize with neural stem cells to enhance spinal cord injury repair via regulating microenvironment and facilitating nerve regeneration. *Adv Healthc Mater*. 2023;12(18):e2300123. doi: 10.1002/adhm.202300123

184. Sun H, Xu J, Wang Y, et al. Bone microenvironment regulative hydrogels with ROS scavenging and prolonged oxygen-generating for enhancing bone repair. *Bioact Mater*. 2023;24:477-496.
doi: 10.1016/j.bioactmat.2022.12.021

185. Hu C, Huang R, Xia J, et al. A nanozyme-functionalized bilayer hydrogel scaffold for modulating the inflammatory microenvironment to promote osteochondral regeneration. *J Nanobiotechnol*. 2024;22(1):445.
doi: 10.1186/s12951-024-02723-x

186. Zhao Z, Xia X, Liu J, et al. Cartilage-inspired self-assembly glycopeptide hydrogels for cartilage regeneration via ROS scavenging. *Bioact Mater*. 2024;32:319-332.
doi: 10.1016/j.bioactmat.2023.10.013

187. Liu Z, Wang T, Zhang L, et al. Metal-phenolic networks-reinforced extracellular matrix scaffold for bone regeneration via combining radical-scavenging and photo-responsive regulation of microenvironment. *Adv Healthc Mater*. 2024;13(15):e2304158.
doi: 10.1002/adhm.202304158

188. Zhao LL, Luo JJ, Cui J, et al. Tannic acid-modified decellularized tendon scaffold with antioxidant and anti-inflammatory activities for tendon regeneration. *ACS Appl Mater Interfaces*. 2024;16(13):15879-15892.
doi: 10.1021/acsami.3c19019

189. Xue H, Zhang Z, Lin Z, et al. Enhanced tissue regeneration through immunomodulation of angiogenesis and osteogenesis with a multifaceted nanohybrid modified bioactive scaffold. *Bioact Mater*. 2022;18:552-568.
doi: 10.1016/j.bioactmat.2022.05.023

190. Deng C, Zhou Q, Zhang M, et al. Bioceramic Scaffolds with Antioxidative Functions for ROS scavenging and osteochondral regeneration. *Adv Sci (Weinh)*. 2022;9(12):e2105727.
doi: 10.1002/advs.202105727

191. Zhou T, Xiong H, Wang SQ, et al. An injectable hydrogel dotted with dexamethasone acetate-encapsulated reactive oxygen species-scavenging micelles for combinatorial therapy of osteoarthritis. *Materials Today Nano*. 2022;17:100164.
doi: doi: 10.1016/j.mtnano.2021.100164

192. Pan Y, Cao S, Terker AS, et al. Myeloid cyclooxygenase-2/prostaglandin E2/E-type prostanoid receptor 4 promotes transcription factor MafB-dependent inflammatory resolution in acute kidney injury. *Kidney Int*. 2022;101(1):79-91.
doi: 10.1016/j.kint.2021.09.033

193. da Silva Morais A, Oliveira JM, Reis RL. Small animal models. *Adv Exp Med Biol*. 2018;1059:423-439.
doi: 10.1007/978-3-319-76735-2_19

194. Liu TP, Ha P, Xiao CY, et al. Updates on mesenchymal stem cell therapies for articular cartilage regeneration in large animal models. *Front Cell Dev Biol*. 2022;10:982199.
doi: 10.3389/fcell.2022.982199

195. McIlwraith CW, Frisbie DD, Kawcak CE, Fuller CJ, Hurtig M, Cruz A. The OARSI histopathology initiative - recommendations for histological assessments of osteoarthritis in the horse. *Osteoarthritis Cartilage*. 2010;18(Suppl 3):S93-105.
doi: 10.1016/j.joca.2010.05.031

196. McCoy AM. Animal models of osteoarthritis: comparisons and key considerations. *Vet Pathol*. 2015;52(5):803-818.
doi: 10.1177/0300985815588611

197. Proffen BL, McElfresh M, Fleming BC, Murray MM. A comparative anatomical study of the human knee and six animal species. *Knee*. 2012;19(4):493-499.
doi: 10.1016/j.knee.2011.07.005